APPLICATIONS OF MACHINE LEARNING STRATEGY FOR WIRELESS POWER TRANSFER AND IDENTIFICATION

A Dissertation
Presented to
The Academic Faculty

By

Soyeon Jeong

In Partial Fulfillment
of the Requirements for the Degree
Doctor of Philosophy in the
School of Electrical and Computer Engineering

Georgia Institute of Technology

May 2020

Copyright © Soyeon Jeong 2020

APPLICATIONS OF MACHINE LEARNING STRATEGY FOR WIRELESS POWER TRANSFER AND IDENTIFICATION

Approved by:

Dr. Manos M. Tentzeris, Advisor
School of Electrical and Computer Engineering
Georgia Institute of Technology

Dr. Andrew F. Peterson
School of Electrical and Computer Engineering
Georgia Institute of Technology

Dr. Gregory D. Durgin
School of Electrical and Computer Engineering
Georgia Institute of Technology

Dr. Sangkil Kim
Department of Electronics Engineering
Pusan National University

Dr. Yang Wang
School of Civil and Environmental Engineering
Georgia Institute of Technology

Date Approved: April 20 , 2020

To my family and friends

ACKNOWLEDGEMENTS

I would like to express my deepest gratitude to my advisor, Dr. Manos Tentzeris for his guidance and generous support. It is my greatest honor and pleasure to work under his supervision for my Ph.D. research. I would like to thank my proposal and defense committee members, Dr. Andrew Peterson, Dr. Gregory Durgin, Dr. Sangkil Kim, and Dr. Yang Wang for their thoughtful feedback and suggestions on my thesis. Also, I would like to thank Dr. Myungsuk Jo, Dr. Rui Ma, former and current ATHENA group members and friends for their support. Lastly, I want to express my sincerest gratitude to my family for being so supportive of me over all these years. Although they have been far, they always supported me and encouraged me to finish my Ph.D.

TABLE OF CONTENTS

LIST OF TABLES

LIST OF FIGURES

LIST OF SYMBOLS AND ABBREVIATIONS

ε_{r}	Dielectric constant (Permittivity)
$\varepsilon_{\mathrm{eff}}$	Effective dielectric constant
λ	Wavelength
Ω	Ohm
μ_0	Permeability
A	Ampere
ADS	Advanced Design System
ANN	Artificial Neural Networks
CMT	Coupled Mode Theory
dB	Decibels
dBm	dB power relative to mW
DC	Direct Current
EM	Electromagnetics
GHz	Giga Hertz
HF	High Frequency
IL	Insertion Loss
IoT	Internet of Things
k-NN	k-Nearest Neighbor
LDA	Linear Discrimination Analysis
MHz	Mega Hertz

μH	Micro Henry
ML	Machine Learning
mm	Millimeter
MRC	Magnetic Resonance Coupling
MSE	Mean Square Error
nH	Nano Henry
NN	Neural Networks
OOK	On-Off Keying
pF	Pico Farad
PPM	Pulse Position Modulation
PTE	Power Transfer Efficiency
RF	Radio Frequency
RFID	Radio Frequency Identification
SAW	Surface Acoustic Wave
SVM	Support Vector Machine
TDR	Time Domain Reflectometry
UAV	Unmanned Aerial Vehicle
UWB	Ultra Wide Band
VHF	Very High Frequency
VNA	Vector Network Analyzer
WPT	Wireless Power Transfer

SUMMARY

The objective of my research is to propose and demonstrate Machine Learning (ML) applications of wireless power transfer and identification technology. Several works describe the implementation of a ML strategy based on 1) the use of Neural Networks (NN) for real-time range-adaptive automatic impedance matching of Wireless Power Transfer (WPT) applications, 2) the Naive Bayes algorithm for the prediction of the drone's position, thus enhancing the WPT efficiency, and 3) the Support Vector Machine (SVM) classification strategy for read/interrogation enhancement in chipless RFID applications.

The ML approach for the effective prediction of the optimal parameters of the tunable matching network, and classification range-adaptive transmitter coils (Tx) is introduced, aiming to achieve an effective automatic impedance matching over a wide range of relative distances. A novel WPT system consisting of a tunable matching circuit and 3 Tx coils which have different radius controlled by trained NN models is characterized. A proof-of-concept WPT platform which allows the accurate prediction of the drone's position based on the flight data utilizing ML classification using the Naive Bayes algorithm is also given. A ML-based approach for classification and of detection tag IDs has been presented, which can perform effective transponder readings for a wide variety of ranges and contexts, while providing high tag-ID detection accuracy. A SVM algorithm was trained using measurement data, and its accuracy was tested and characterized as a function of the included training data. In summary, this research sets a precedent, opening the door to a rich and wide area of research for the implementation of ML methods for the enhancement of WPT and chipless RFID applications.

CHAPTER 1

INTRODUCTION AND BACKGROUND

In early 1889, Nikola Tesla invented the Tesla coils [1], which can transfer power wirelessly based on the magnetic resonance and near-field coupling of resonators, as shown in Figure 1.1. Compared to the traditional method of wire-powered, wireless power transmission introduces many benefits as follows: 1) Hassle from the connecting cable is removed, which can be user-friendly. 2) Smaller devices without the attachment of batteries can be designed and fabricated. 3) Without having regularly plug or unplug, it provides better product durability for contact-free devices. 4) It may not be cost-effective to replace the batteries or connect the cables when it is costly, hazardous, or infeasible. Starting from this, numerous research on wireless power transfer (WPT) began. WPT can be radiative or non-radiative, depending on the energy transfer mechanisms. Radiative WPT, based on the electromagnetic waves, adopts RF/microwave typically radiation as a medium to deliver energy in the long-range with low power region. Non-radiative WPT is based on the coupling of the magnetic field between two coils within the distance of the coils' dimension for power transmission and characterized by near-field range.

1.1 Non-radiative Wireless Power Technology

1.1.1 MRC System Architectures

Before the evolution of resonant coupling, inductive coupling technique for wireless charging was the most common and popular technology [2]. This technique can be very efficient when the primary and secondary coils are placed closely to each other (transmis-

(a)

Figure 1.1: University of Illinois student Steve Ward and Fermilab senior technician Jeff Larson developed twin Tesla coils capable of emitting 12 feet (4 meters) of sparks. (Image: © Fermilab)

sion distance limited to few centimeters) and carefully aligned, which means the magnetic coupling between two coils must be large enough to operate properly. However, inductive coupling techniques are only suitable for high power transmission within a very short range since the transmission efficiency between two coils is easily affected by the variations of angular, axial, and lateral misalignment in the inductive coupled system.

The potential breakthrough in WPT is the development of the highly resonant techniques using a magnetic field to transfer energy over a mid-range distance of 2 meters by the MIT team [3]. This technology is referred to as "magnetic resonance", and it is often contrasted to "inductive" for its ability to efficiently transfer power over a range of distances and with misalignment. The theory of resonant coupled WPT is based on the principle that two resonators tuned at the same resonant frequency can effectively transfer energy with greater efficiency at a longer power transmission distance compared to inductive coupling techniques. The power transmission in resonant coupled WPT system can be done either by using loosely coupled or strongly coupled coils. Actually, the high quality (Q) factor

of coils makes the energy coupling strong which can successfully compensate for the efficiency degradation caused by the low couplings. The Q factor of the antenna is described by equation (1.1)

$$Q = L/r \tag{1.1}$$

when L is the inductance of coil antenna and r is the resistance of coil.

Diverse Magnetic Resonance Coupling (MRC) system architectures are utilized in the near-field WPT, which can facilitate the impedance matching to optimize the system transfer characteristics. The WPT system with two-coil resonators has been established with the analysis of mutual coupling between two resonant circuits [4] and [5]. The WPT system architectures with three and four coils also have been proposed, which can optimize the transfer characteristics with additional adjustment freedom degrees. A three-coil architecture was introduced in [7] based on Coupled Mode Theory (CMT), using the fundamental principle underlying their physical mechanism, which is similar to the known Electromagnetically Induced Transparency (EIT) process. This system architecture can improve the transfer power with an assumption had been made that the mutual inductance M_{23} and M_{34} could be adjusted simultaneously in Figure 1.2-(b). The four-coil architecture reported in [3], which involves a power driving coil, a sending resonator, a receiving resonator, and a load coil, provides three mutual coupling coefficients M_{12}, M_{23} and M_{34} as shown in Figure 1.2-(c). These mutual coupling coefficients can be utilized to maximize the power transfer when it can meet the condition: $(M_{12} \cdot M_{34})/M_{23} = 1$. Several works [8], [9], have transformed the analysis using electric circuit theory while the CMT is used in [3].

Moreover, the WPT system architecture with multi-relay coils [10]-[11] can not only extend the transfer distance without change of efficiency but improve system energy effi-

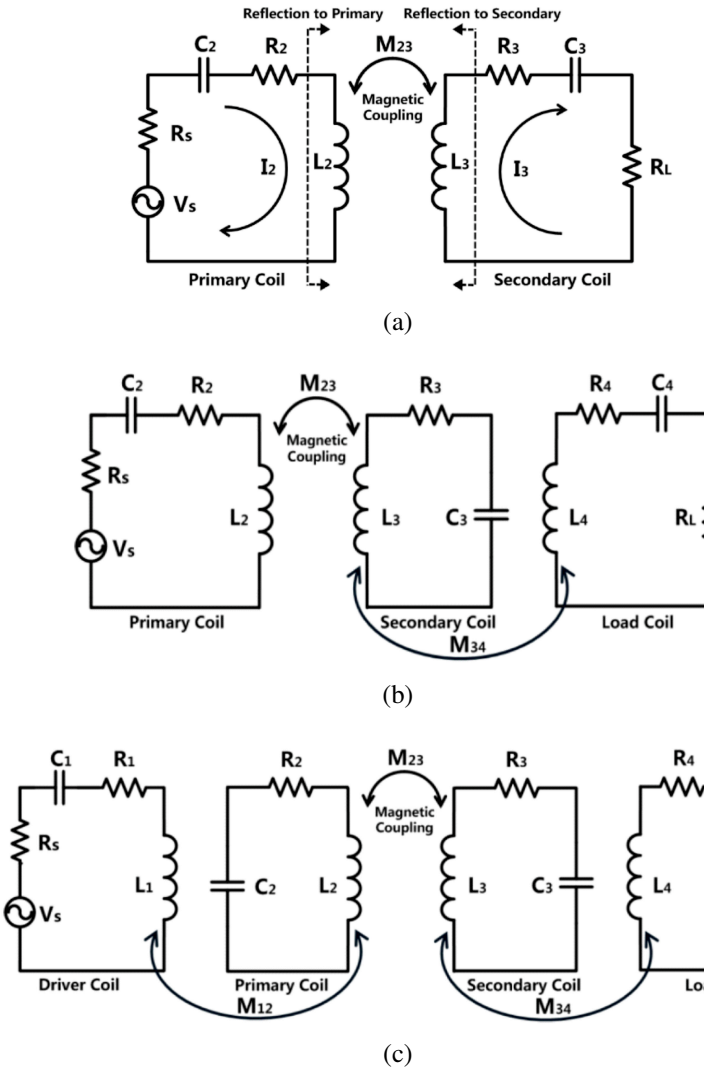

Figure 1.2: (a) Equivalent circuit model of the two-coil WPT system. (b) Equivalent circuit model of the three-coil WPT system. (c) Equivalent circuit model of the four-coil WPT system [6].

ciency. One of the systems with multi-relay coils has been studied in [10], considering the analysis of the transfer characteristics of the system based on CMT, and it is shown that efficiency is improved in the cases of not only a coaxially but also a perpendicularly arranged intermediate system [11]. Recently, wireless domino-resonator systems have been investigated [12]-[13], which are flexible systems that allow the coil-resonators to be placed in various domino forms arranged coaxially, non-coaxially, and circularly as shown in Figure 1.3. By using meta-material, an artificial arrangement of identical unit cells, for WPT

system architecture [14], they are able to improve the mutual coupling strength and, therefore, power efficiency. Besides, a WPT system with multi-transmitter and multi-receiver coils [15] has been proposed that can improve the overall efficiency of power transfer by increasing the number of receiver coils.

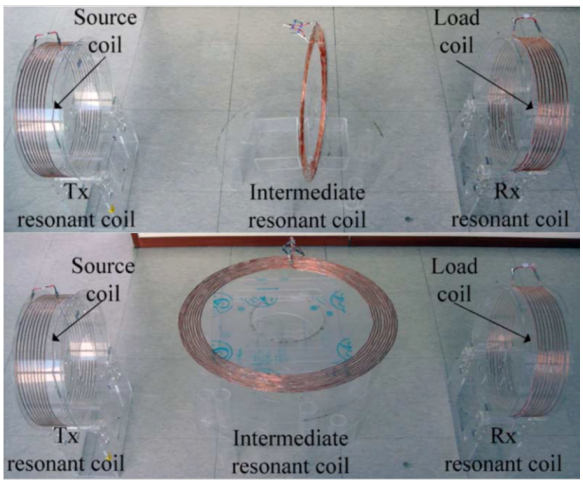

(a)

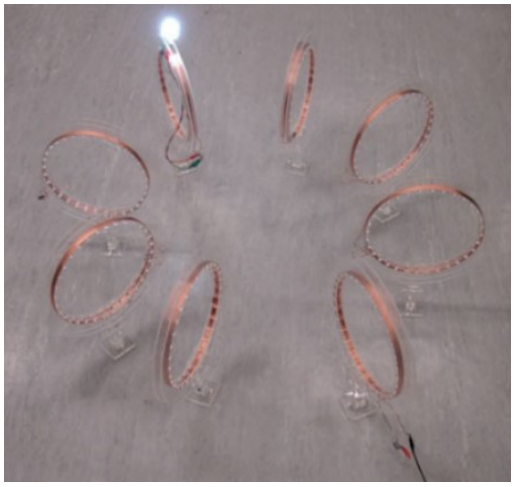

(b)

(c)

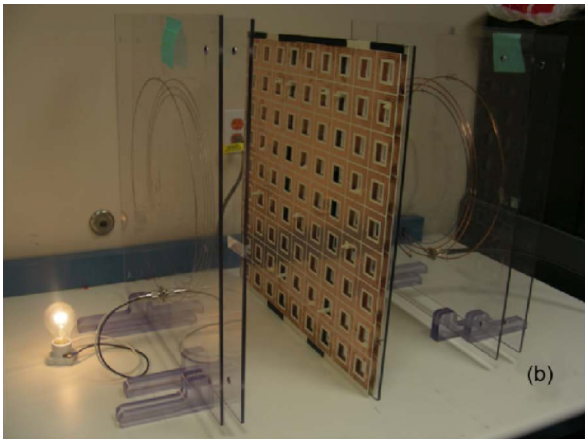

(d)

Figure 1.3: (a) Coaxially and perpendicularly arranged intermediate-resonator system [11]. (b) Circular domino-resonator system [16]. (c) Straightly domino-resonator system [13]. (d) The use of metamaterials and array of coupled resonators [14].

1.1.2 Impedance Matching

The impedance matching of a WPT system using MRC has become a critical challenge in order to maintain a reasonable PTE for time-varying configurations. Various MRC system architectures are utilized in the near-field WPT, which can facilitate impedance matching to optimize the system transfer characteristics. At this point, the frequency splitting phenomenon is a key issue that happens in the over coupled area with multi-coil systems, such as multi-relay coils, multi-transmitter coils, and multi-receiver coils, related to the power transfer efficiency and capability of the WPT system. In other words, there will be an impedance mismatch between the resonator impedance and load impedance by changing the distance, orientation, or misalignment. To overcome this issue, the adaptive frequency tracking procedures [17], [18] have been used which can achieve maximum power delivery, but only operating in a wide bandwidth which is typically outside of the narrow industrial, scientific, and medical frequency bands. As the importance of robustness against distance variation in the WPT system becomes greater, the authors [19], [20] proposed an impedance matching technique based on the characteristic of changing the distance between the coils physically. By adjusting the relative distances or angles between adjacent coils based on the optimal coupling factor between the source and the internal resonator [19], a high-efficiency WPT system is achieved without any lossy matching network. The adaptive system [20] with the reconfigurable resonant coil system, which consists of a series of subcoils that use switches to control the number of turned-on subcoils, increased the efficient transfer range. Similarly, an analytic design method for impedance-matched WPT systems using an arbitrary number of coils by applying flexible coil positioning has been proposed in [21]. Moreover, [22] recently proposed the digital programmable transmitter coils to maximize system efficiency in WPT systems when a receiver coil is given.

In [23] and [24], a tunable matching circuit was designed for a range-adaptive WPT system with switching capacitors to obtain wide tunability from the impedance matching circuit. When the input impedance of a WPT system changed with the distance, a tunable matching circuit can be used to match the variable impedance with the distance. The L-type or inverted L-type matching network placed in the transmitter side is used in [23], and the π-type network placed in both the transmitter and receiver sides is used in [24] with the number of relays, inductors, and capacitors for switching. Besides, a range-adaptive WPT system utilizing multi-loop topology uses a tunable matching network composed of varactors in [25]. In previously reported work [26], we utilized the Genetic Algorithm (GA) to optimize the matching circuit design over a wide range of impedances, and therefore, WPT efficiency is potentially high. Recently, an automatic impedance matching technique based on the feedforward-backpropagation (BP) neural network has been proposed [27] to maintain a PTE at a reasonable level. However, these are limited in the effective ranges as a consequence of their unexpected variation of the transfer distance or load impedance.

For the application, WPT systems can be used not only over a short-range in offices and homes to charge different electric devices such as smartphones, PCs, tablets, and audio players [28] but over a mid-range to charge electric trams and vehicles [29]. Additionally, the importance of WPT systems for moving objects such as a human body for biomedical applications and the Unmanned Aerial Vehicle (UAV) is increasing. In biomedical applications, the capsule type of power supply for diagnosis gastroenterologists [30] and other implantable devices under the human skin [31] has been studied. Also, the WPT systems for UAV applications can improve the battery lifetime to extend the working range without changing the battery, which is used in monitoring crops [32], for example.

1.2 Radiative Wireless Technology

RFID technology is a rapidly growing wireless technology used to track and identify objects using HF, UHF, and RF waves automatically [33]. HF RFID systems are short-range systems based on inductive coupling between the reader and tag antenna through a magnetic field. UHF and microwave RFID systems are long-range systems that use electromagnetic waves propagating between the reader and tag antennas. With the RFID reader, which is known as an interrogator, the RFID transponder, the data encoded and transmitted by RFID tag [34]. However, the cost of traditional tags with a silicon integrated circuit or chip is typically high for many applications involving low-cost items despite featuring significant advantages such as longer reading distances, high capacity of data storage, and the ability to read multiple tags simultaneously. The design and fabrication of application specific integrated circuits (ASICs) needed for RFID are the major component of their cost, which is the main challenge to their adoption. To address this challenge, a printable chipless RFID tag [35], which uses materials that reflect a portion of the reader's signal back, with a unique return signal that can be used as an identifier, was developed by using low-cost conductive inks. Mainly, printable chipless RFIDs are a particularly appealing solution in contexts where cost is one of the most relevant constraints, as reported in [35].

1.2.1 Chipless RFID

Different technologies for data encoding in chipless RFID tags can be classified based on the information encoding techniques: time domain reflectometry (TDR)-based tags and spectral signature-based (frequency-based) tags. In the time domain techniques, different types of methods are used; Surface Acoustic Wave (SAW), On-Off Keying (OOK) modulation, and Pulse Position Modulation (PPM). Printable TDR-based chipless tags encode

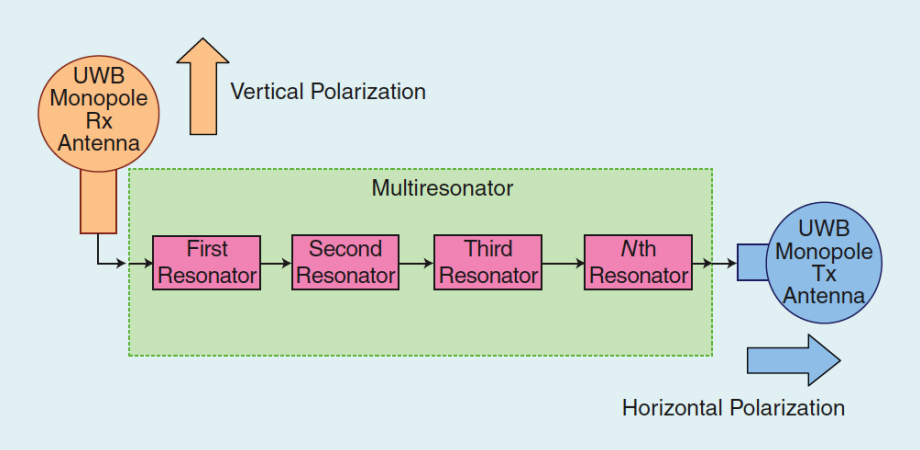

Figure 1.4: Chipless RFID tag including the receiving and transmitting UWB antennas, reprint from [38].

information by following the backward echoes of the pulse sent from the reader [36]. After that, the tag sends echo pulses to the reader after a short time and with some time delays, which is called the backscattered signal. Some advantages include; long reading range [37], orientation-independent to the reader, and robustness to environmental clutter.

Typically, chipless-RFID tags are based in the frequency domain, implemented with multi resonant elements tuned at different, and predefined, frequencies, and are equipped with a transmitting and receiving antenna cross-polarized to communicate wirelessly with the reader, as shown in Figure 1.4. As depicted in Figure 1.5, such antennas are used for the reception of the interrogation signal and the transmission of the spectral signature of the tag. The frequency signature-based tag, which is one of the methods used for communicating the stored tag-ID data, encodes the resonances in the frequency domain and then transforms the frequency spectrum of an interrogation signal transmitted by an RFID reader to communicate the data bits contained in the tag. Since the tag-ID detection process is challenging with the characteristics of the data for decoding the tag-ID data, the importance of several detection techniques for the accurate and robust extraction of data bits has been increased.

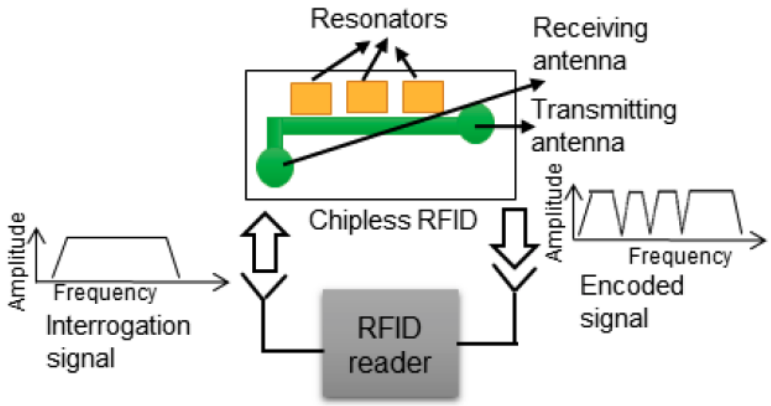

Figure 1.5: Complete block diagram of the chipless RFID tag operation principle, reprint from [39].

In [40]-[41], to improve upon the fixed threshold levels derived from the calibration tag applied to identify and detect the tag-ID, the moving average technique is added in advance. The concept of signal space representation for the detection of tag-ID is introduced and developed in [42]. This approach is capable of estimating the resonant properties of a chipless tag without using calibration tags and without additional signal processing up to a distance of 30 cm. Phase response information of a chipless RFID tag is used for detection of the tag-ID in [43] by representing in a set of prolate spheroidal wave functions. A hybrid coding technique by combining phase deviation and frequency position encoding is proposed in [44] with the metallic strip resonators. This work demonstrated the possibility of using more than one physical dimension to control two coding parameters. Recently, the chipless RFID tag detection technique utilizing a pattern recognition approach to verify document originality was proposed [45]. In their system, there is no need to use particular tags and substrates if the backscatter signal is strong enough under the test. To better understand, a comparison of the chipless RFID tag-ID detection techniques in the frequency domain is shown in Table 1.1.

Table 1.1: CHIPLESS RFID TAG-ID DETECTION TECHNIQUES IN FREQUENCY DOMAIN I

Reference	Tag type	Detection Technique	Frequency (GHz)	Distance (cm)
[40]	Spiral resonator	Threshold detection	1.9-2.5	10
[46]	Multi-spiral resonator	Threshold detection with moving average	2-10	5-40
[47]	Multi-patch resonator	Signal space representation (SSR)	0-8	up to 30
[43]	Spiral resonator	Second derivative of the phase response	3.9-4.5	10
[44]	Metallic strip resonator	Phase deviation and frequency positioning encoding	2.5-7.5	up to 50
[45]	Alphabetic	Frequency scanning pattern recognition	57-64	10-16

1.3 Machine Learning Strategy

Over the past decade, ML algorithms have been deployed in many applications such as prediction, forecasting, diagnostics, etc. New problems to utilize ML are allowed by rapidly increasing processor speed and access to huge-scale data sets. As this rise of ML applications continues, it is useful for large and wide datasets with similar or closely related. Also, ML algorithms that have been trained to identify specific information can achieve this in considerably less time rather than a manual analysis which is impractical and inefficient. Thus, when exposed to a large dataset, ML enables applications to determine the best course of action or procedure that will deliver the best result in the shortest time by detecting the pattern and using historical and real-time data. By taking this advantage of the ML techniques, solutions to the problems of Wireless power transfer and identification technologies are explored.

1.4 Thesis Outline

This thesis is organized in the following way:

1. Chapter 2 provides the background of ML classification techniques by addressing their processes and relative advantages in detail.

2. Chapter 3 demonstrates ML applications for the WPT systems, including the automatic real-time range-adaptive impedance matching network.

3. Chapter 4 presents the design and performance of ML application for the WPT systems in UAV localization.

4. Chapter 5 demonstrates ML applications for the chipless RFID system in read/interrogation enhancement.

5. Chapter 6 discusses the conclusion and contribution.

CHAPTER 2

MACHINE LEARNING STRATEGY

As discussed briefly in the previous chapter, ML techniques have been successfully applied to numerous challenging problems having drastically improved the efficiency of the designed systems and the design of machines. Commonly, there are two types of ML algorithms: "supervised" learning and "unsupervised" learning, and specific groupings are shown in Figure 2.1. One algorithm of learning called "supervised" is useful in cases where instances are given with a known dataset (the training dataset) corresponding to the certain dataset in which prediction can later be made [48]. In other words, "supervised" learning requires that the data used to train the algorithm is already labeled with correct answers while "unsupervised" learning uses neither classified nor labeled data to group unsorted information according to similarities, patterns, and differences with no prior training. The trained model first is trained to produce a function of supervised learning algorithm and then uses a test dataset to validate the model. Based on the training dataset containing instances, classification could identify which of a set of categories a new instance belongs. Typically, the majority of practical ML uses "supervised" when instances are given with known labels corresponding to correct output. The analysis of the trained data and produced a function of "supervised" learning algorithm, which operates with two main tasks, regression and classification, can be used for mapping new instances.

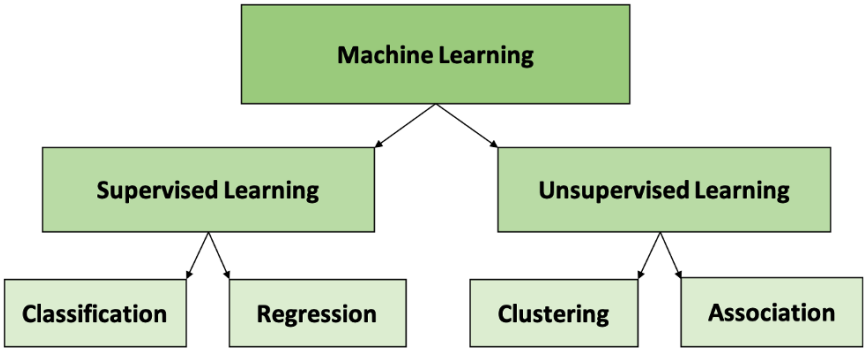

Figure 2.1: Different groupings of machine learning.

2.1 Classification

Many classification methods have been widely applied to numerous challenging problems to make predictions or calculated suggestions based on large amounts of data. Classification methods aim at identifying the category of a new observation among a set of categories on the basis of a labeled training set. From the literature [49], five potential classification approaches were identified: Decision Trees (DT), k-Nearest Neighbor (k-NN), Linear Discriminant Analysis (LDA), Naive Bayes, and Support Vector Machine (SVM). Their processes and relative advantages and disadvantages are detailed below.

2.1.1 Decision Trees

The DT is a widely used method for classification and regression problems that is based on the form of a tree structure [50], as shown in Figure 2.2. It breaks down a dataset into smaller subsets while at the same time, an associated decision tree is incrementally developed from three nodes, namely root node, internal node, and leaf node. As described in [51], a decision tree is a structure in which each root node presents the entire sample and

this further gets divided into two or more homogeneous sets, each internal node represents a "test" on an attribute, and each branch represents the outcome of the test. Each leaf node represents a class label. Tree-based methods typically empower predictive models with the advantages of being simple to understand and interpret while providing relatively inaccurate outcomes with instability. This method is easy to understand and interpret which closely mimics the human decision-making process. Also, DT is very suitable for a non-parametric model with no assumptions about the shape of data despite the fact that it tends to overfit easily.

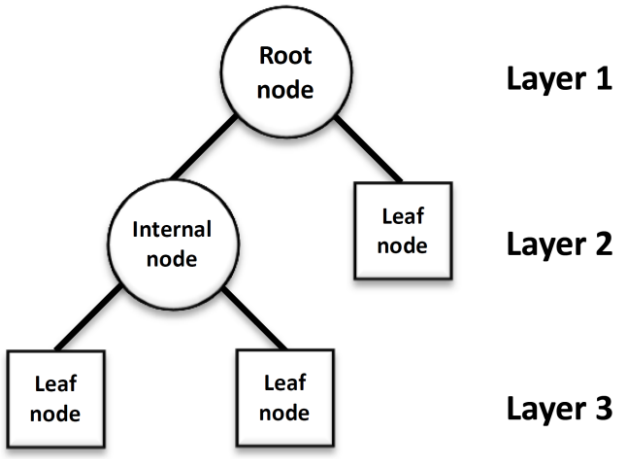

Figure 2.2: Basic structure of a DT, reprint from [52].

2.1.2 k-Nearest Neighbor

The k-NN algorithm is one of a simple instance-based learning algorithm for prospective statistical classification [53]. When an instance with an unknown class is presented for evaluation, the algorithm computes its k closest neighbors, and assign the class by voting among those k neighbors. To determine which of the k instances in the training dataset are most similar to a new input a distance measure is used. For real-valued input variables, the most popular distance measure is Euclidean distance (2.1). Euclidean distance is calculated

as the square root of the sum of the squared differences between feature vectors A=(x_1, x_2, x_3,...,x_N) and B=(y_1, y_2, y_3,...,y_N) where N is the dimensionality of the feature space.

$$distance(A, B) = \sqrt{\frac{1}{N}\sum_{i=1}^{N}(x_i - y_i)^2} \tag{2.1}$$

As we increase the value of k, the predictions become more stable due to majority voting and averaging to make more accurate predictions. Figure 2.3 shows the basic example of

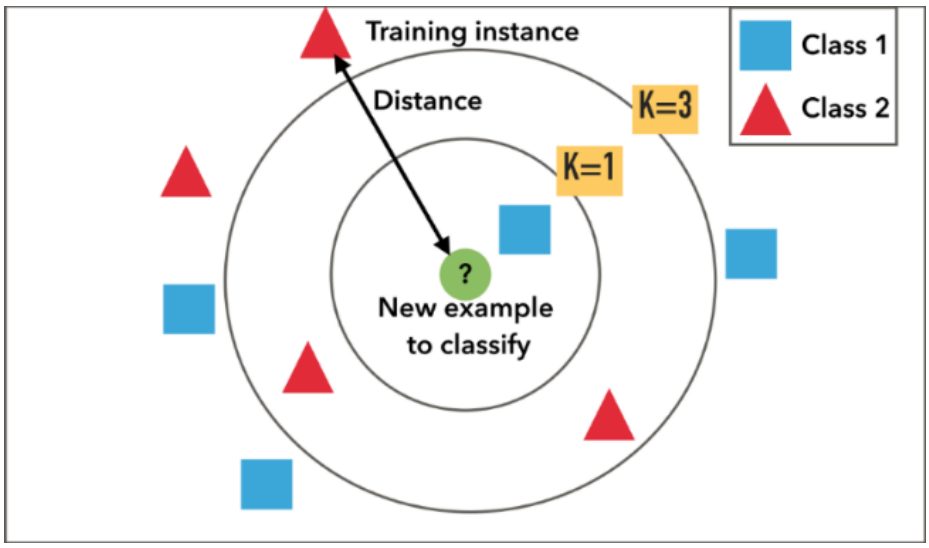

Figure 2.3: k-NN Classification, reprint from [54].

k-NN classification. The test sample (inside circle) should be classified either to the first class of blue squares or to the second class of red triangles. If k = 3 (outside circle), it is assigned to the second class because there are 2 triangles and only 1 square inside the inner circle. If for example k = 5, it is assigned to the first class (3 squares vs. 2 triangles outside the outer circle). k-NN is called "lazy learner" because it does not learn anything in the training period. In other words, it does not derive any discriminative function from the training data resulting in much faster speed than other algorithms that require training.

2.1.3 Linear Discriminant Analysis

The LDA is a dimensionality reduction technique that is commonly used for supervised classification problems [55]. DA makes predictions by finding linear combinations of predictor variables that best separate the groups of observations, called discriminant functions. Suppose there are k different groups, each assumed to have a multivariate normal distribution with mean vectors $\mu_k(k = 1, 2, .., k)$ and common covariance matrix $\sum$. The actual mean vector and covariance matrices are almost always unknown; the maximum likelihood estimates are used to estimate these parameters. The idea of LDA is to classify observations x_i to the group k, which minimizes the within-group variance.

$$\text{k} = \arg\min_k (x_i - \mu_k)^T \sum^{-1} (x_i - \mu_k) \tag{2.2}$$

LDA works when dealing with categorical independent variables for each observation are continuous quantities under the assumption that there must be a statistically significant difference in the mean vectors between groups, and the number of observations in each group must be greater than the number of predictors. If any one of these assumptions is not met, the results may be unreliable.

2.1.4 Support vector machine

The SVMs have been applied to various classification problems such as development prediction models with high success [56]. The SVM essentially constructs a set of $(N-1)$ dimensional hyperplanes in N-dimensional space to separate data points into groups used for classification, as shown in Figure 2.4. When given a training dataset of n points of the form $\overrightarrow{x}_n, y_n$ where the y_i are either 1 or -1 indicating the class to where the point $\overrightarrow{x}_i$

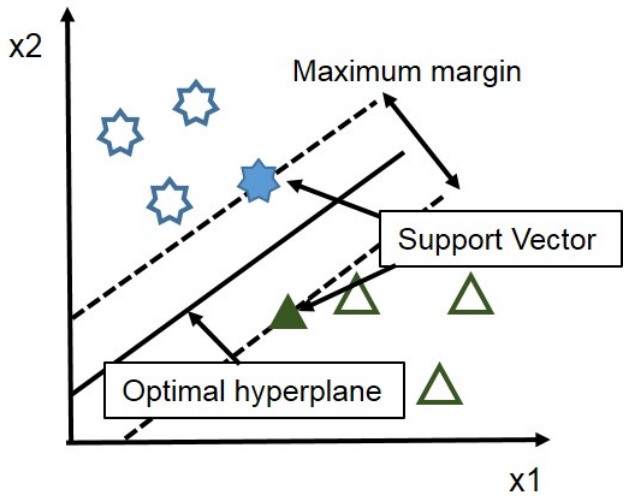

Figure 2.4: Basic concept of SVM classification.

belongs, any hyperplane can be written as the set of points $\overrightarrow{x}$ satisfying $\overrightarrow{w} \cdot \overrightarrow{x} - b = 0$ where $\overrightarrow{w}$ is the normal vector to the hyperplane and the parameter $b/\overrightarrow{||w||}$ determines the offset of the hyperplane. In this respect, the optimal separating hyperplane for which the margin is maximum is essential to place unseen test points far away from the hyperplane or in the margin. By employing a polynomial kernel function (2.3) of a hyperplane, the points x in the d-dimensional feature space that are mapped into the hyperplane are defined by a relation such as $\sum_i a_i k(x_i, x)$ making it easy to compute the similarity in the original space.

$$k(x_i, x_j) = (x_i^T \cdot x_j + c)^d \tag{2.3}$$

The final decision function is given by (2.4) for new predictions, which takes a dataset as input and gives a decision as output.

$$f(x) = sign \sum_{i}^{n} (a_i y_i) k(x_i, x_j) + b \tag{2.4}$$

The SVM classifiers are trained on the entire training set using the optimized parameters and evaluated for their performances on the test sets with kernel scales, which is the free parameter invariant and independent of the input dimension. Several types of the kernel functions with different kernel scales can be used in the training process, depending on the applications.

2.1.5 Naive Bayes Classification

Naive Bayes is a simple yet effective and commonly-used, machine learning classifier. It is a probabilistic classifier that makes classifications using the Maximum A Posteriori (MAP) decision rule in a Bayesian setting that can also be represented using a straightforward Bayesian network. Also, the Naive Bayes algorithm predicts the various sets of probabilities based on the condition values in particular classes. The Bayes theorem provides a way of calculating the posterior probability, $P(C_k|x)$, from the prior probability of class, $P(C_k)$, the likelihood which is the probability of predictor given class, $P(x|C_k)$, and the prior probability of predictor $P(x)$.

$$P(C_k|x) = \frac{P(C_k)P(x|C_k)}{P(x)} \tag{2.5}$$

$$P(x|C_k) = \prod_{i=1}^{n} P(x_i|C_k) \tag{2.6}$$

$P(x|C_k)$ is the conditional probability of seeing the evidence x if the hypothesis C_k is true. For any unseen test data, the method computes the posterior probability of that sample belonging to each class, then classifies the test data according to the largest posterior

probability, as shown in equation (2.7).

$$y = \underset{k \in \{1,2,\ldots,K\}}{\arg\max} P(C_k) \prod_{i=1}^{n} P(x_i|C_k) \tag{2.7}$$

Naive Bayes classification is a particularly appealing method in contexts where speed is one of the most relevant constraints. However, there is a limitation with the real-world application of this classifier because of the assumption that all features are independent which is not usually the case.

2.2 Neural Network Classification

Artificial Neural networks (ANNs) represent powerful machine learning-based techniques, inspired by the neurons in the human brain as shown in Figure 2.5, that are designed to recognize patterns or underlying relationships in a set of data. They consist of the input layer, multiple hidden layers, and an output layer connected with every node. The layers between the input layer and output layers are known as hidden layers, as the training data does not show the desired output for these layers. A given node takes the weighted sum of its input and passes it through a non-linear activation function,

$$z = f(b + x \cdot w) = f(b + \sum_{i=1}^{n} x_i w_i) \tag{2.8}$$

where x_i is input parameter, w_i is weight factor, and b is bias which is an additional parameter used to adjust the output along with the weighted sum of the inputs to the neuron. An NN turns out to be well-suited to modeling high-level abstractions across a wide array of disciplines and industries including computer vision, speech recognition, machine translation, and even in activities that have traditionally been considered as reserved to humans

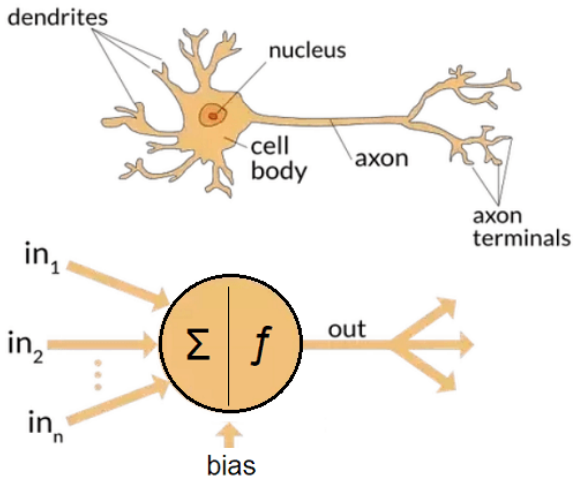

Figure 2.5: Neural network classification, reprint from [57].

[58]. The main advantage of an NN lies in its ability to outperform nearly every other ML classification algorithms, but this goes along with the disadvantages that users don't know how and why an NN came up with a certain output, known as "black box" nature, compared to other interpretable algorithms.

Overall, there is no one ML classification approach or one solution that caters to all types of problems. In other words, it is hard to know which algorithm will work best because the type and kind of data and application play a crucial role in the algorithm is performance. It is common to consider the ML algorithms identified as potentially useful approaches, throw your data into them, run them all in either parallel or serial, and at the end evaluate the performance of the algorithms to select the best one. So it becomes more important to explain why a certain mode is best suited in a particular situation, and Figure 2.6 demonstrates the typical trend of interpretability comparison between the ones that are most relevant to the use cases under consideration in this work among the many other algorithms.

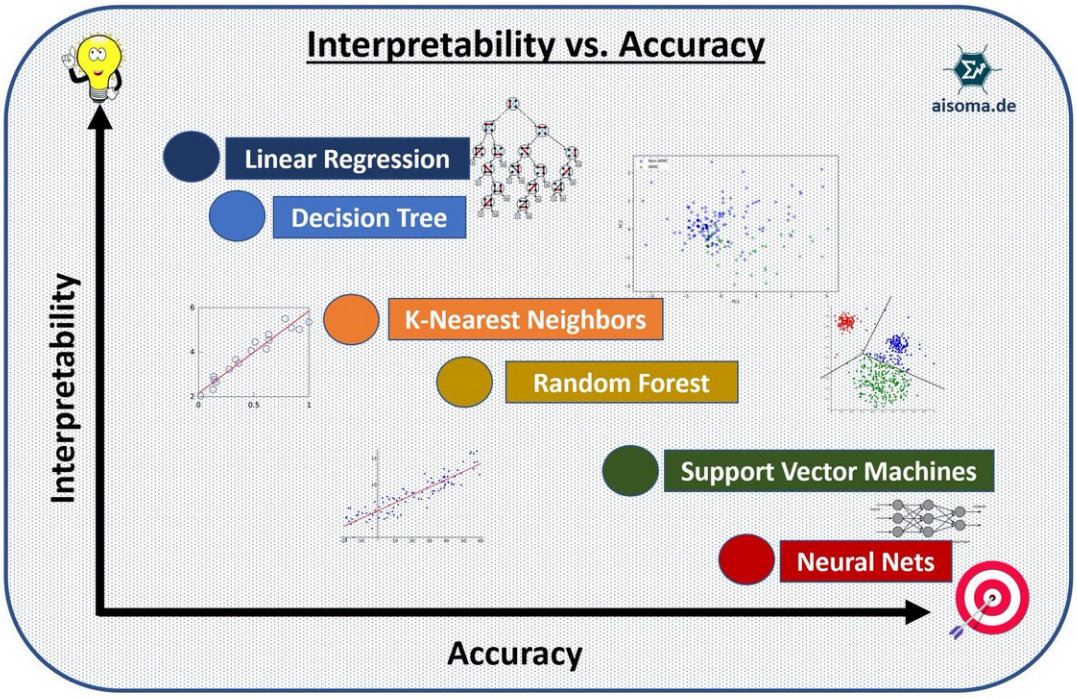

Figure 2.6: The model interpretability comparison between ML classification methods, reprint from [59].

CHAPTER 3

A REAL-TIME RANGE-ADAPTIVE IMPEDANCE MATCHING UTILIZING A MACHINE LEARNING STRATEGY BASED ON NEURAL NETWORKS

3.1 Introduction

As reviewed in chapter 1, the impedance matching of a WPT system using MRC has become a critical challenge in order to maintain a reasonable Power Transfer Efficiency (PTE) for time-varying configurations. Several approaches of impedance matching have been proposed [60], [61] and [26] regarding the distance between the receiver (Rx) and transmitter (Tx) as PTE varies significantly with distance. However, these are limited in the effective ranges as a consequence of their unexpected variation of the transfer distance or load impedance. In this chapter, an alternative approach is proposed that takes advantage of a novel method based on a feedforward NN technique, thus addressing the shortcomings of the aforementioned impedance matching approaches while retaining high PTE. As a proof-of-concept, one receiver coil, three selective transmitter coils and a matching circuit with tunable capacitors are first designed and measured. Then, an ML approach utilizing NN algorithms that can construct the mapping relationship is presented to improve the capability of the WPT system.

3.2 WPT Application

3.2.1 Matching Circuit Design and Fabrication

A matching circuit topology consisting of 3 consecutive L-type series inductors and shunt capacitors with p-i-n diode switches was used in [26], and it was fabricated on a 1.5 mm thick substrate, RO4003C, which features a dielectric constant (ε_r) of 3.38, provided by Rogers Cooperation. The simplified schematic of this matching circuit is shown in Figure 3.1-(a), and a fabricated prototype is shown in Figure 3.1-(b).

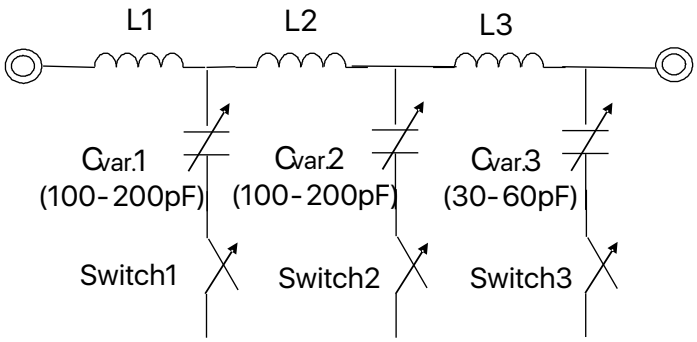

(a)

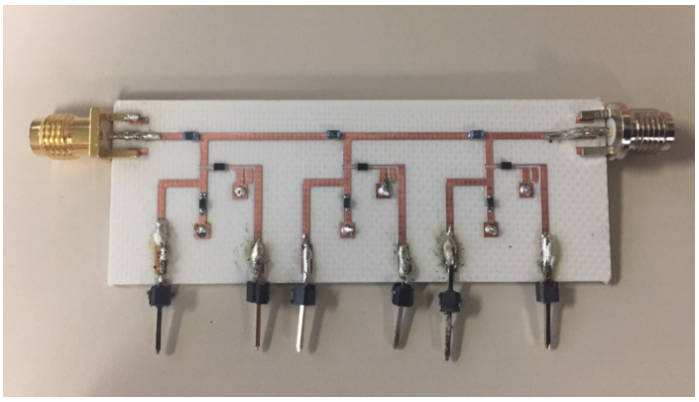

(b)

Figure 3.1: Simplified schematic of the automatic matching circuit.

To overcome the limited capability of this static topology to provide an acceptable PTE over a wide range of transmitter-receiver distances, one variable capacitor from Murata electronics is employed in this design enabling a superior characteristic of matching cir-

cuit compared with previous work and allowing for on-demand tuning utilizing the results from the proposed machine learning approach. These tunable capacitors typically achieve capacitance values that can vary by applying voltage to their electrodes in the range of 100 pF-200 pF (0-5 V) for $Cvar.1$ and $Cvar.2$, 30 pF-60 pF (0-3 V) for $Cvar.3$ and operate appropriately at 13.56 MHz with the limited range of values. As experimental verification of the variability of the capacitance values is shown in Figure 3.2.

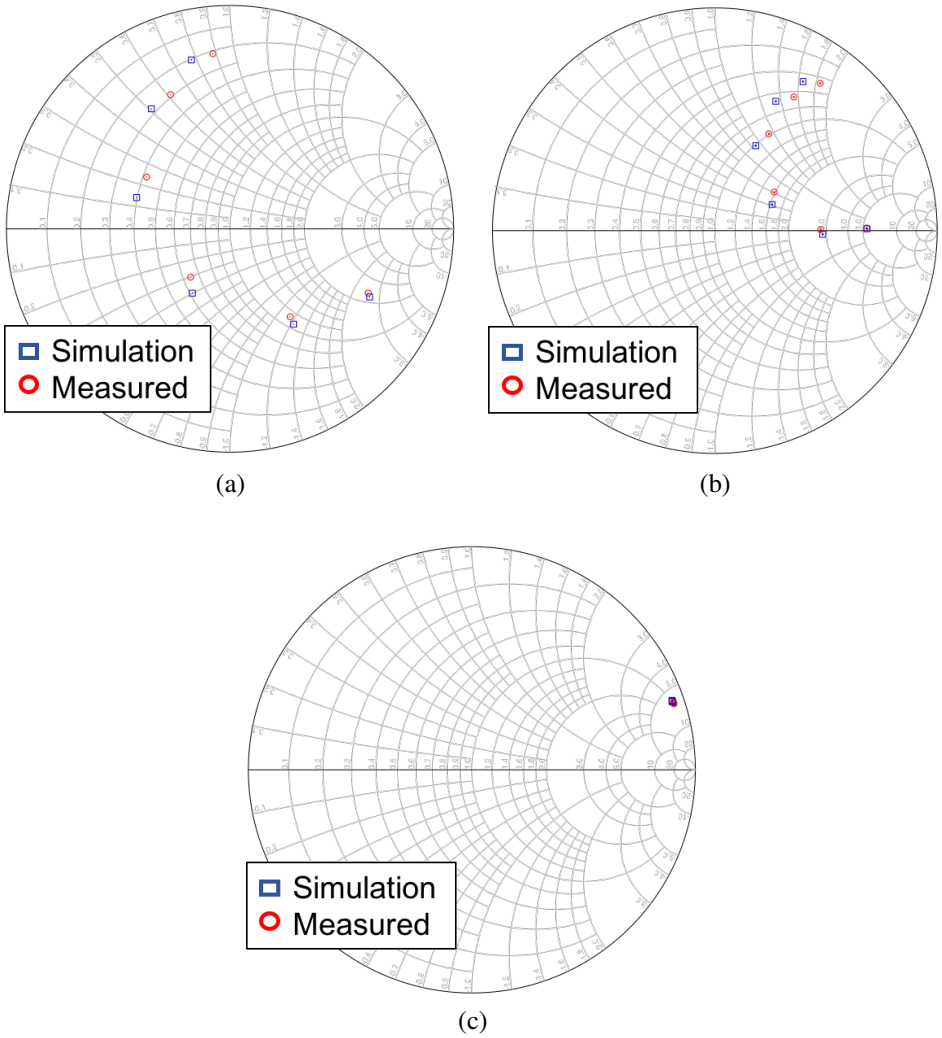

Figure 3.2: Simulated and Measured capacitance variability of (a) Cvar.1 (b) Cvar.2 (c) Cvar.3.

In order to determine the optimal matching circuit topology with those tunable capacitors, the impedance matching coverage of multiple topologies, π-type and L-type segments of multiple sections (1 to 3 consecutive stages) with each section comprising of a series inductor, a shunt capacitor, and a switch were simulated with respective matching impedance coverage ranges shown in Figure 3.3. The impedance matching coverage was verified for a range of the capacitance values of $Cvar.1$ (100-200 pF), $Cvar.2$ (100-200 pF), and $Cvar.3$ (30-60 pF) in steps of 10 pF. The reason for using 10 pF steps of the capacitance values is to satisfy the practical control module constraints in a system implementation. Since the power transfer to the load can be maximized when the input impedance of the matching circuit looking from port.2 (Z_{22}) in Figure 3.1 is the complex conjugate of the Rx-Tx coil topology impedance input (Z_c), each fixed inductor value of $L1$, $L2$, $L3$, and the use of capacitor among $Cvar.1$, $Cvar.2$, and $Cvar.3$ were first optimized to minimize the reflection coefficient $\Gamma = (Z_c^* - Z_{22})/(Z_c^* + Z_{22})$ from the simulated coil configuration (Rx-Tx1, Rx-Tx2, and Rx-Tx3) impedance values (Z_c) at distances of 10, 15, and 20 cm. The 3 consecutive stage L-type topology was chosen to provide wide impedance matching coverage and satisfy the practical constraints such as the loss associated with the lumped circuit components. With this proposed method, a wide range of impedance coverage can be realized though the variation of the input impedance Z_{in}. For the inductance values of $L1$, $L2$, and $L3$, the fixed inductor values 1432 nH, 610 nH and 1484 nH were optimized corresponding to the values of capacitance's tunable ranges in simulations utilizing Advanced Design System (ADS) 2016. For the fabrication of a proof-of-concept prototype of the matching circuit, a 1.5-mm-thick substrate from RO4003C provided by the Rogers Cooperation and inductors with fixed values of 1500 nH and 560 nH provided by the Coilcraft 0603HL series were used.

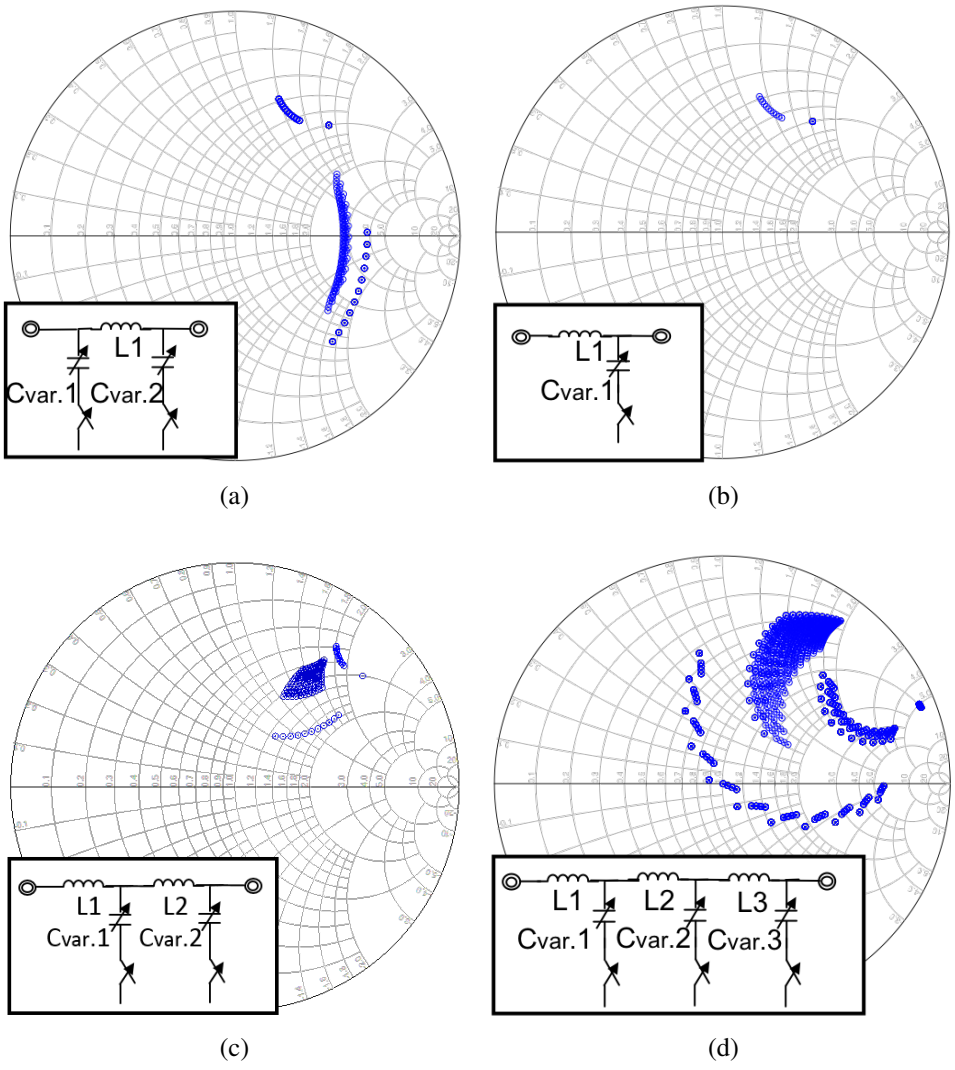

Figure 3.3: (a) Simulated input impedance values of π-type matching circuit with Cvar.1 and Cvar.2. (b) Simulated input impedance values of 1 L-type matching circuit with Cvar.1. (c) Simulated input impedance values of 2 L-type matching circuit with Cvar.1 and Cvar.2. (d) Simulated input impedance values of 3 L-type matching circuit with Cvar.1, Cvar.2, and Cvar.3.

3.2.2 Receiver and Selective Transmitters Configurations

Both receiver and transmitter coils are open-type helical coils which have a self-resonance frequency of 13.56 MHz. For proof-of-concept purpose, each coil is designed with given radius (r=5 cm for the Receiver, 10, 15 and 20 cm for the transmitters) to resonate at the same frequency by optimizing the number of turns and the gap between each coil wires using the CST studio 2016 integral solver. Simulated and measured results for the reflection coefficient of one receiver coil are shown in Figure 3.4. A multi transmitter coil topology is employed to reduce the variation in the input impedance of the WPT system with respect to the distance. In order to maximize the coil-to-coil efficiency, it was found that the optimal radius of Tx is approximately equal to the distance of coil-to-coil [22], thus we obtain the analytically derived (3.1)

$$r_{Tx} = d \tag{3.1}$$

when $r_{Rx} << r_{Tx}$. Based on their analysis, the overall geometrical design for Rx and Tx coils is controlled by the key parameters summarized in Table 3.1.

To improve the robustness of the both coil structures, laser cut acrylic boards were use as support fixtures. The extracted S-parameters from the simulations will serve a standard

Table 3.1: PARAMETERS OF THE RX AND TX COILS FOR THE PROPOSED WPT SYSTEM

	Receiver	Transmitters		
	Rx	Tx1	Tx2	Tx3
Self-resonance Frequency (MHz)	13.56			
Copper Wire Radius (mm)	0.5			
Radius (cm)	5	10	15	20
Number of turns	27	10	6	4.5
Pitch (mm)	2			

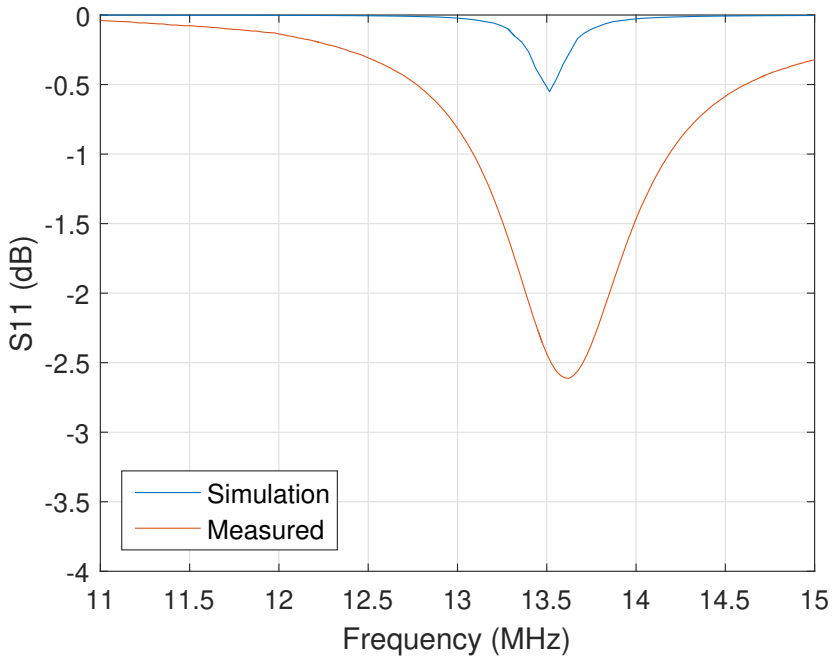

Figure 3.4: Simulated and measured the reflection coefficient of one receiver coil.

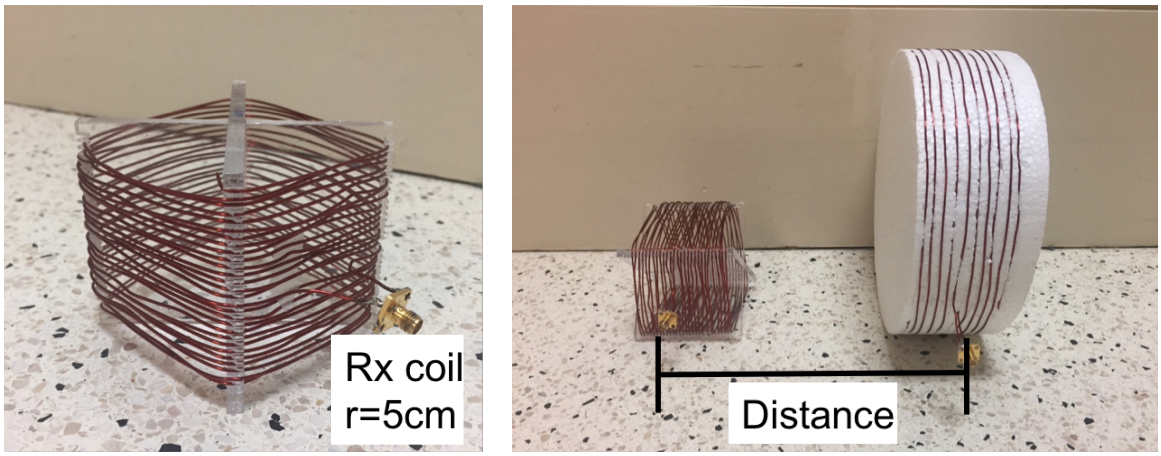

(a) (b)

Figure 3.5: (a) Fabricated Rx coil. (b) Distance between Rx and Tx1.

dataset for the NN training presented in the next section. A photograph of the fabricated 3 Tx coils in both stacked and aligned placement are shown in Figure 3.8.

In order to confirm the effectiveness of this approach, several open type helical coils with different radius were designed on CST studio 2016 using the integral solver. The ex-

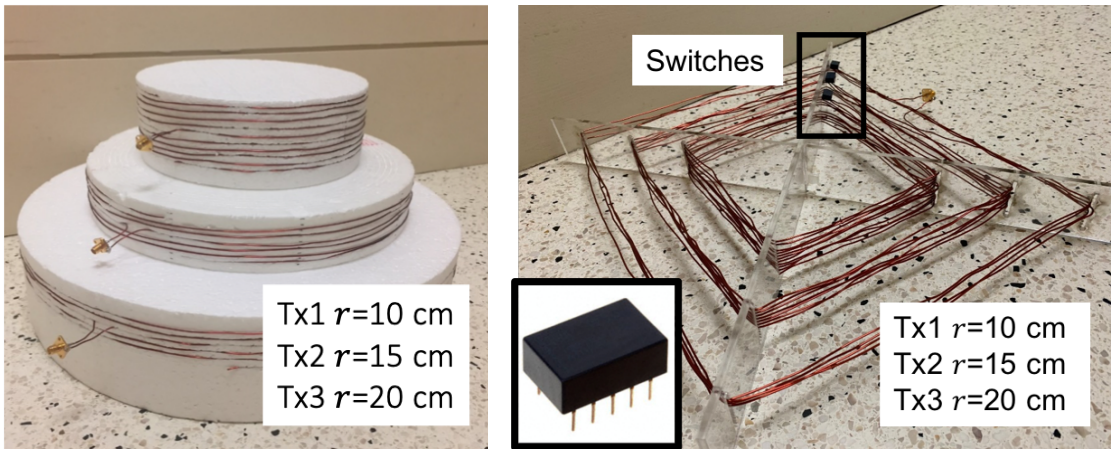

(a) (b)

Figure 3.6: (a) Stacked fabricated 3 Tx coils. (b) Aligned fabricated 3 Tx coils with switches.

tracted S-parameters from the simulations will serve a standard dataset for the NN training presented in next section. A photograph of the fabricated Rx and Tx coils are shown in Figure. 3.6. Each switch introduces a selectivity of the transmitter coils by utilizing a relay, TQ2-L2-4.5V from Panasonic Electric works, with an resistance of less than 50 mΩ. In order to confirm the effectiveness of this approach, the reflection coefficient (S_{11}) was simulated according to the coil-to-coil (Rx-Tx1, Rx-Tx2, and Rx-Tx3) distance at 10-25 cm as shown in Figure 3.7. 10 cm is the minimum possible center to center separation distance between Rx-Tx coils since the thickness of the support fixtures are 10 cm for Rx and 8 cm for Tx coils. The multi transmitter coil topology can be effectively used in the range-adaptive WPT system in addition to use of the proposed tunable matching circuit.

3.2.3 Mutual Inductance of the Selective Tx

Mutual inductance of the selective Tx coils is one of the challenging issues of this multi selective coil configuration, which is the interaction of one coil magnetic field on another coil as it induces a voltage in the adjacent coil. The mutual inductance that exists between

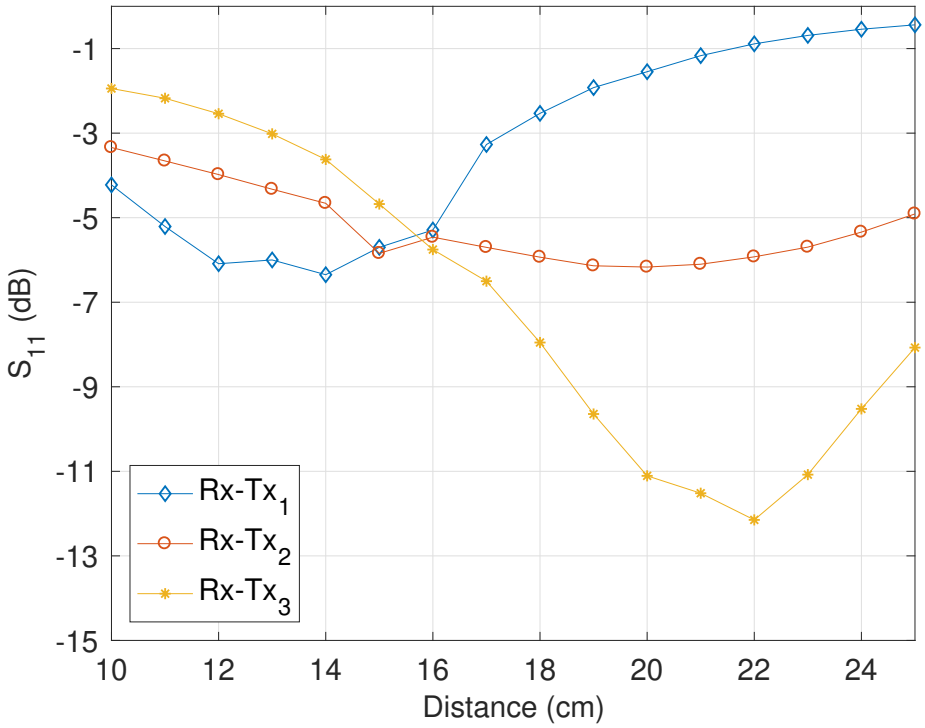

Figure 3.7: Simulated reflection coefficient (S_{11}) with respect to Rx-Tx distances.

the two coils can be greatly increased by positioning or by increasing the number of turns of either coil as would be found in a transformer, as given in (3.2) where μ_0 is the permeability of free space, μ_r is the relative permeability of the soft iron core, N is the number of coil turns, A is in the cross-sectional area in m^2, and l is the length of the coil in meters.

$$M = \frac{\mu_0 \mu r N_1 N_2 A}{l} \tag{3.2}$$

Figure 3.8 shows the simulated reflection coefficient when three coils are in stacked placement with the calculated mutual inductance M_{21}=M_{12}= 4.94 uH, M_{13}=M_{31}= 2.89 uH, M_{23}=M_{32}= 4.11 uH, and in aligned placement with the calculated mutual inductance M_{21}=M_{12} = 6.74 uH, M_{13}=M_{31}= 4.69 uH, M_{23}=M_{32}= 5.77 uH. Since strong mutual inductance between 3 coils in both conditions is desired for the practical scenario, each parameter of the

coil is re-optimized to resonate at 13.56 MHz considering the status of the switch with their placement as shown in Figure 3.9.

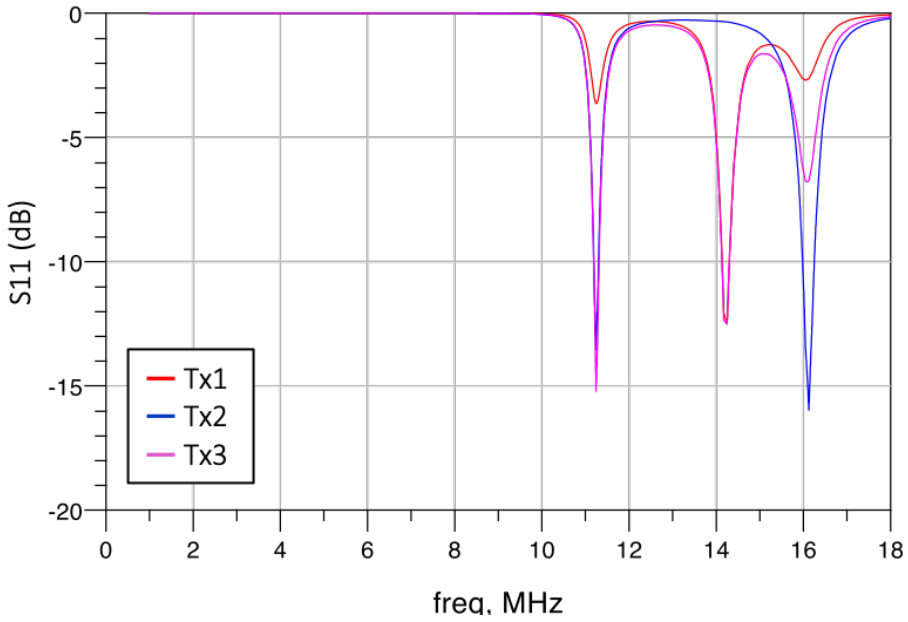

(a)

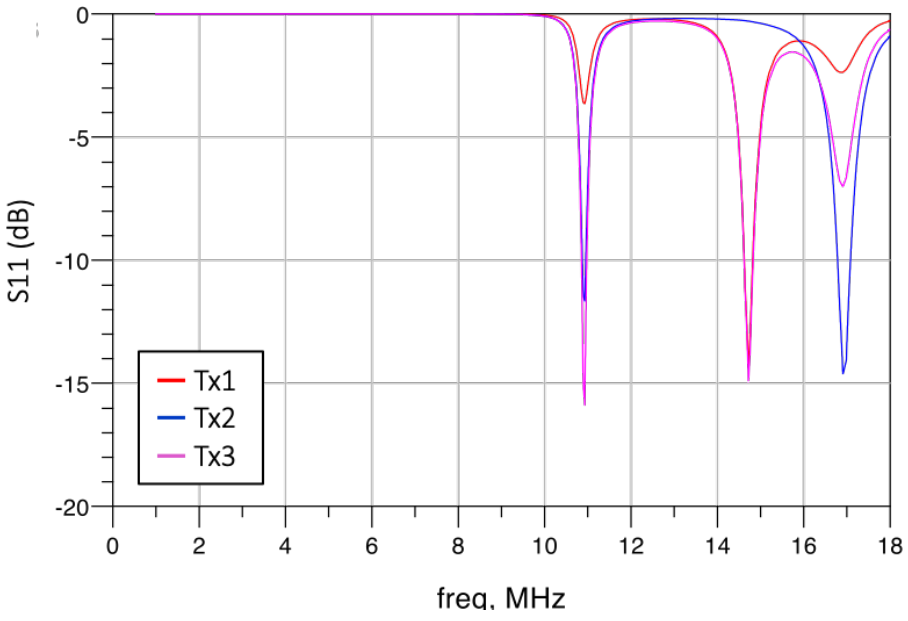

(b)

Figure 3.8: (a) Simulated reflection coefficient (S_{11}) when three coils are in stacked placement. (b) Simulated reflection coefficient (S_{11}) when three are in aligned placement.

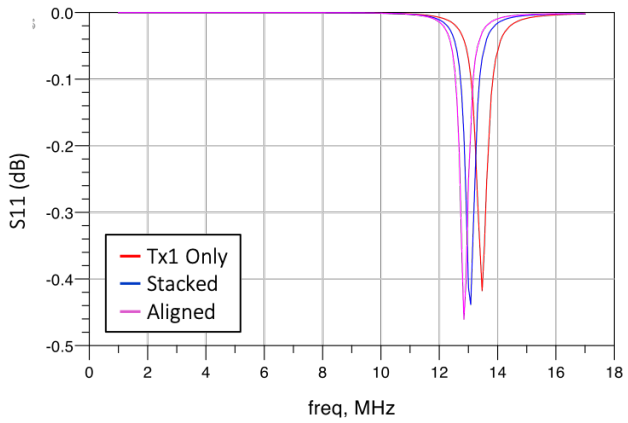

(a)

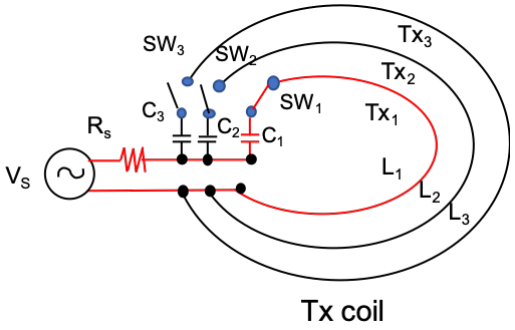

(b)

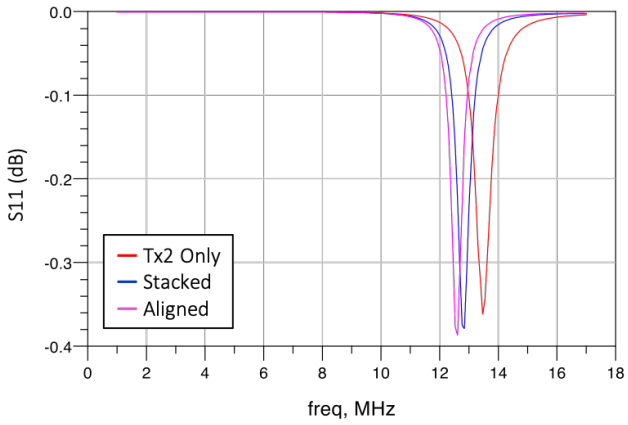

(c)

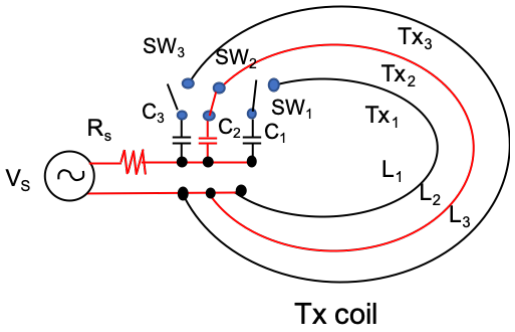

(d)

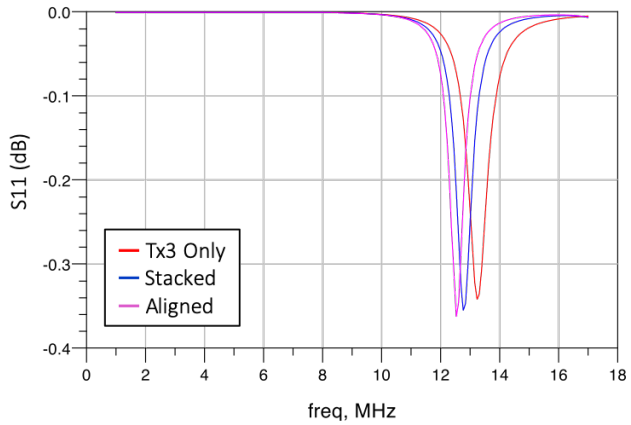

(e)

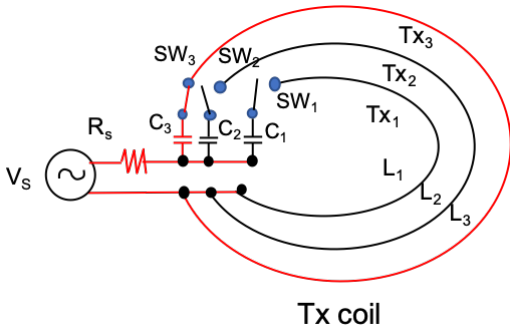

(f)

Figure 3.9: (a) Simulated reflection coefficient (S_{11}) after re-optimization when the Tx1's switching status "ON". (b) Tx coil schematic when the Tx1's switching status "ON". (c) Simulated reflection coefficient (S_{11}) after re-optimization when the Tx2's switching status "ON". (d) Tx coil schematic when the Tx2's switching status "ON". (e) Simulated reflection coefficient (S_{11}) after re-optimization when the Tx3's switching status "ON". (f) Tx coil schematic when the Tx3's switching status "ON".

3.3 Machine Learning Approach

As discussed in the chapter 2, NNs represent powerful machine learning-based techniques, inspired by the neurons in the human brain, that are designed to recognize patterns or underlying relationships in a set of data. These networks turn out to be well-suited to modeling high-level abstractions across a wide array of disciplines and industries. The MATLAB NN toolbox was used to construct suitable NNs with optimal structure parameters.

3.3.1 Optimize the Hyperparameters of the Neural Network

In an ML strategy, the hyperparameters are the variables which determine the network structures and how the network is trained. NNs can have many hyperparameters which are usually set before the training process, such as the number of hidden layers, the number of epochs, and the training function. Hidden layers are the layers between the input layer and output layer, where artificial neurons take in a set of weighted inputs and produce an output through an activation function. It is a typical part of nearly any NN in which engineers simulate the types of activity that go on in the human brain. While stacking many hidden layers allows us to learn more complex relationships in the data, such an approach is also more prone to potentially overfitting data. Also, a validation dataset is a dataset of samples used to provide an unbiased evaluation of a model fit on the training dataset while tuning model hyperparameters. The difference between the validation dataset and the test dataset is that the validation dataset is used to compare competing models, whereas the test dataset is used to evaluate the model by providing the standard. Here, we calculated the Mean

Square Error (MSE) (3.3)

$$MSE = \frac{1}{n}\sum_{i}^{n}(y_i - \widehat{y_i})^2 \tag{3.3}$$

between the desired NN output y_i and the NN output $\widehat{y_i}$, to compare the performance of the trained network with two different hyperparameters: 1) the number of hidden layers and 2) the three training functions (The Levenberg-Marquardt, Bayesian Regularization, and Scaled conjugate gradient). The number of epochs is also one of the hyperparameters of gradient descent that controls the number of complete passes through the training dataset. In other words, an epoch is one learning cycle where the learner sees the whole training dataset. A sufficient number (1000) was used along with each network to avoid having the training MSE stuck in a minimum. Figure 3.10-(a) shows the calculated MSE of the validation data corresponding to the number of hidden layers and Figure 3.10-(b) shows the MSE of the test data corresponding to the number of hidden layers from 5 to 15. In Figure 3.10-(b), the MSE for the Bayesian Regularization function is always zero because of the function that performs Bayesian regularization backpropagation disables the validation stops by default. In other words, this function does not require a validation dataset at the point of checking validation to see if the error on the validation set gets better or worse as training goes on. Since the value of MSE is good when it close to 0, the number of hidden layers used for the NN should be 10 for this application with the Levenberg-Marquardt and Bayesian Regularization functions. We use the following data partitioning methods which have been suggested in most of the related articles: 70% of the entire dataset is used for training, 15% of the entire dataset for validation, and 15% of the entire dataset for testing.

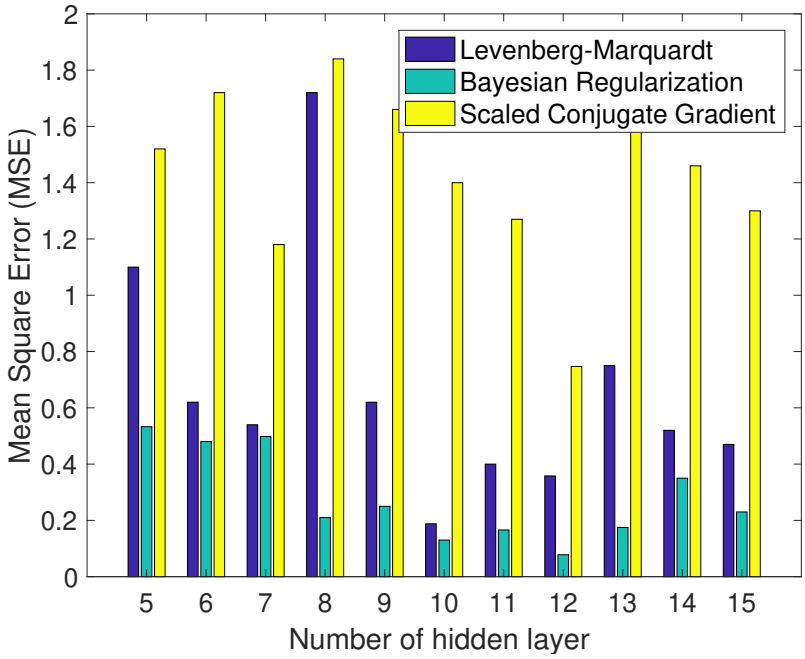

(a)

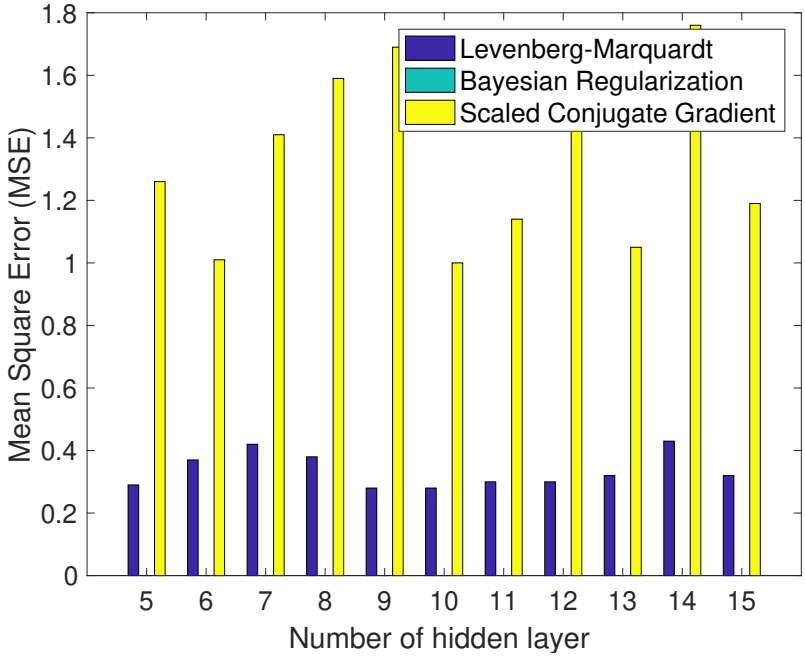

(b)

Figure 3.10: (a) Mean Square Error (MSE) of the test data. (b) Mean Square Error (MES) of the validation data.

3.3.2 Feedforward Neural network with Backpropagation

The feedforward NNs, also called the deep feedforward network, is one of the deep learning models. To approximate some function $f(x)$ through the feedforward NN, when x is input, the feedforward NN defines a mapping function $y = f(x; \theta)$ and determines the parameters θ which gives the best function approximation results [62]. Also, the backpropagation method provides a NN with a set of input values for which the correct output value is known beforehand.

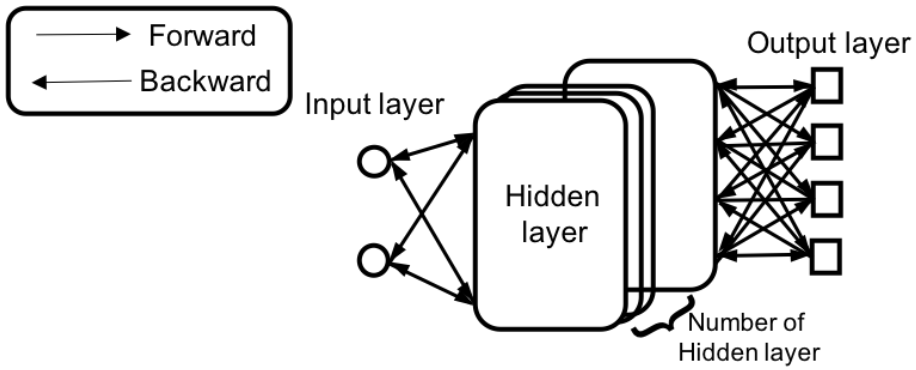

Figure 3.11: The schematic of the feedforward neural network with backpropagation.

In this network as shown in Figure 3.11, the information moves in both directions from the input layers with an associated weight factor (w) to the output layers while the hidden layers are usually used for improving mapping ability. In this work, we propose a WPT scheme with three cascading L-type impedance matching networks based on a feedforward NN, which is a similar approach to that used in [27]. They developed a mapping relationship between the impedance of the equivalent load ($Z_{eq} = R_{eq} + jX_{eq}$) and a matched capacitor set composed of (C_1, C_2) in their Γ-type of matching network. In this work, in consideration of each switch connected to each L-type of matching network, the final out-

put set is composed of (C_1, C_2, C_3). The dataset for training to produce a function of the network consists of the distribution of $|S_{11}|$ matched by the NN within a range of 0 to 20 Ω for R_{eq} and -50 to 50 for X_{eq} with 1 interval (in total 220 datasets). The reason for the use of these dynamic variation ranges of the impedance is based on the consideration of matching range of from small to large variation. In previous work, we proposed the advanced approach using a shallow NN to classify patterns. Through classification, an automated system declares that the input object belongs to a particular category. 220 sets of output parameters, which represent capacitance values (C_1, C_2, C_3) from the above-trained model, act as an input to select the proper single transmitter coil among T_{x1}, T_{x2}, T_{x3}. After that, trained classifier can recognize the three categories associated with each input parameter. In this work, the selection of proper transmitter coils among T_{x1}, T_{x2}, T_{x3} is also included as an output parameter set in consideration of further implementation.

3.4 Implementation and Performance evaluation

3.4.1 Implementation of the Proposed System

Firstly, the trained feedforward NN model is built by the process of the previous section. In order to predict the capacitance values and classify the type of transmitter, a training process using the feedforward NN was implemented. We implemented the trained NN by extracting layer/output weight factors from the MATLAB simulation as the development of the network on Arduino would be the slower process in terms of training time. Before matching, the initial input impedance of Rx-Tx at 13.56 MHz was measured by a vector network analyzer and plotted in Figure 3.12.

To verify the fabricated three transmitters and their selectivity, Figure 3.12 also shows measurement results when one of three transmitter coils was manually selected to achieve

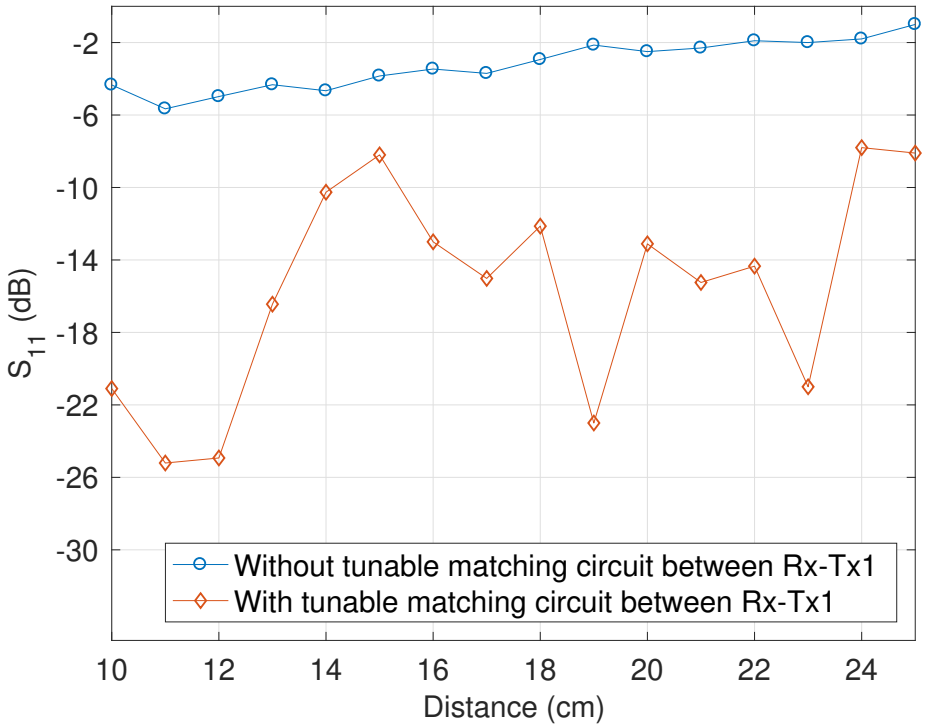
-2
-6
-10
-14
-18
-22
-26
-30
S_{11} (dB)
Without tunable matching circuit between Rx-Tx1
With tunable matching circuit between Rx-Tx1
10
12
14
16
18
20
22
24
Distance (cm)

(a)

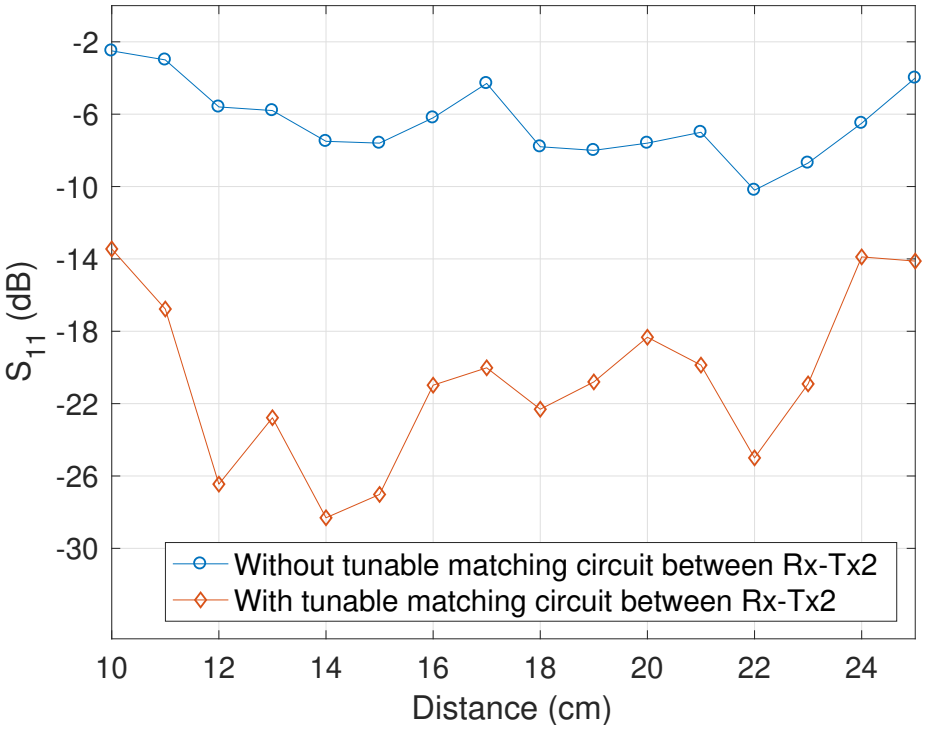
-2
-6
-10
-14
-18
-22
-26
-30
S_{11} (dB)
Without tunable matching circuit between Rx-Tx2
With tunable matching circuit between Rx-Tx2
10
12
14
16
18
20
22
24
Distance (cm)

(b)

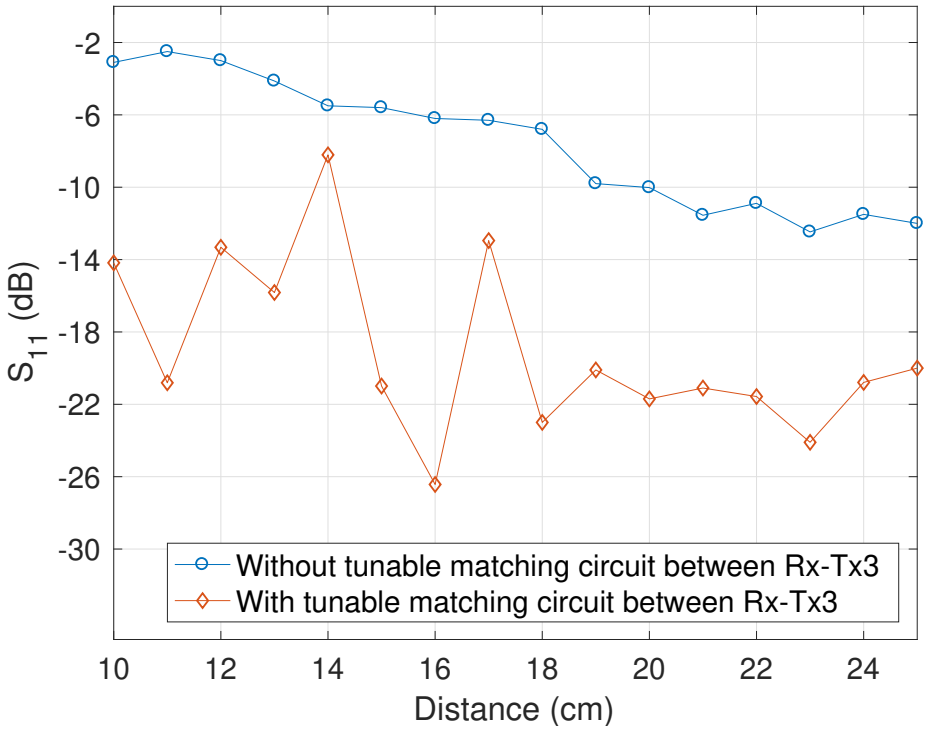

(a)

Figure 3.12: (a) Measured reflection coefficient (S_{11}) with Rx-Tx1. (b) Measured reflection coefficient (S_{11}) with Rx-Tx2. (c) Measured reflection coefficient (S_{11}) with Rx-Tx3.

impedance matching only utilizing the proposed matching circuit depending on each coil-to-coil distance. From the figures, it can be said that classified output parameters, capacitance values (C_1, C_2, C_3), are not accurate at a certain distance because the matched capacitor set was trained with a single transmitter as mentioned in section (3.3.2). This may be the reason why the S_{11} is high at 15 cm in Figure 3.12-(a), and at 14 cm in Figure 3.12-(c). These errors can be prevented by using selective multi transmitters. As discussed in [22], most of each region has a significant improvement according to the coil-to-coil distance such as of Rx-Tx1 at 10-14 cm, Rx-Tx2 at 15-19 cm and Rx-Tx3 at 20-25 cm. Finally, the performance of the proposed approach using combinations of the selective multi transmitters which are controlled automatically, will be discussed in the next section.

3.4.2 Operation Test and Performance Evaluation

To verify the prediction capability for each capacitance value of the impedance matching circuit and the selection capability for multi transmitters, the performance of the entire real-time range-adaptive matching system was tested. The configuration is shown in Figure 3.13.

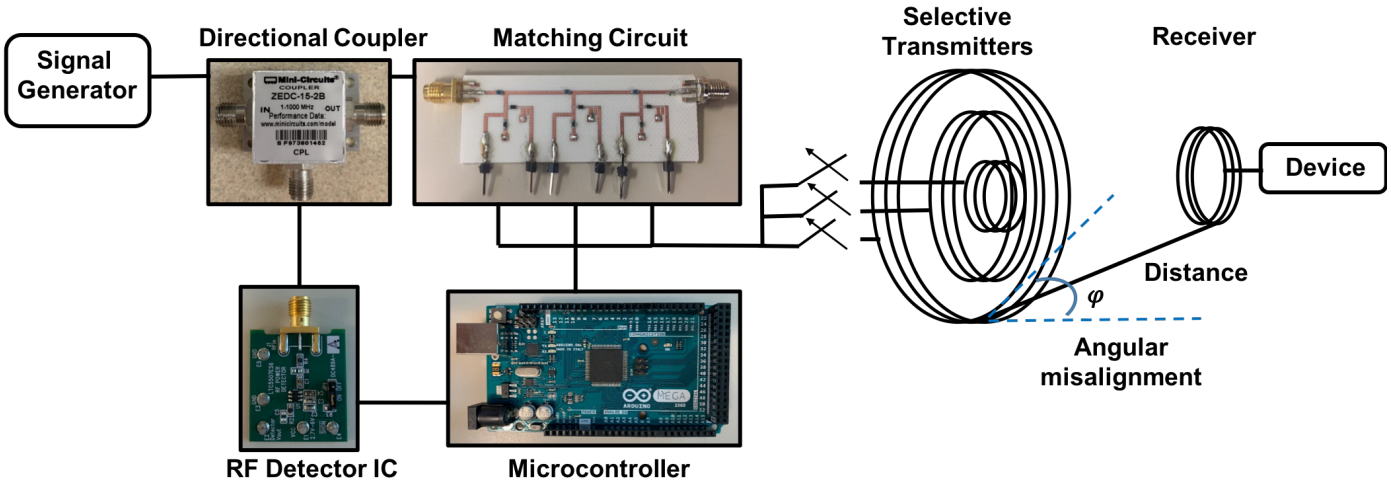

Figure 3.13: Block diagram of the proposed real-time range-adaptive impedance matching WPT system.

Initially, the S_{11} signal is measured by utilizing a directional coupler, ZEDC-15-2B from Mini-Circuits and the RF detector IC, LTC5507 from the Linear Technology Cooperation. Then, the output dc voltage is measured by utilizing an analog-to-digital (ADC) converter in the microcontroller module, not only to calculate the matched capacitor set but to predict the single transmitter through the NN. Finally, the arduino PWM signal is used to drive the voltage to adjust the capacitance values and control the switch in the transmitter selection. In order to verify the validity of the proposed WPT system, the received power at different separation distances was measured by using a real-time spectrum analyzer, RSA3408 from Tektronix Inc., with a tunable matching circuit and multi Tx coils.

The S-parameters of the matched state automatically chosen by the trained NN model at different coil separation distances are measured by utilizing a vector network analyzer, and the extracted value of S_{21} is used to calculate the PTE expressed in (3.4).

$$PTE = |S_{21}|^2 \times 100(\%) \tag{3.4}$$

To verify and validate the proposed approach, Figure 3.14 shows the calculated PTE at each distance in the range of 10 to 25 cm compared with (1) using only one specific Tx coil and (2) with selective Tx coils under the condition of the similar matching approach in [22]. After matching through the trained NN model, the input impedance matching is improved over the entire separation distance range. By utilizing the selective Tx coils, the PTE was more stable and able to avoid the sudden drop at a certain range in both different environments (Case 1: Combined using the manually measured result of the tunable matching circuit, and the multi transmitter coils, respectively. Case 2: Automatically measured results of the entire real-time range adaptive system). Especially at distances 12, 13, 14, 16, 18, 19 and 22 cm, the capacitance values and selected single transmitter coil extracted from the trained NN model results in significant improvement by employing the selective transmitter coils controlled by the trained NN as shown in Figure 3.16. Moreover, the proposed approach achieves a PTE around 90% for ranges within 10 to 25 cm.

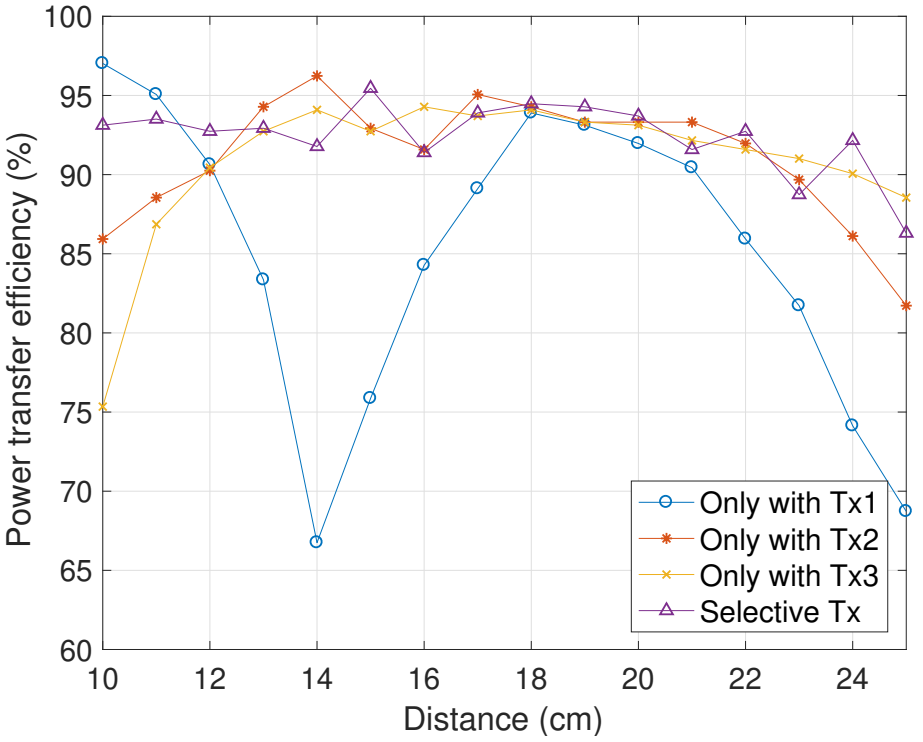

(a)

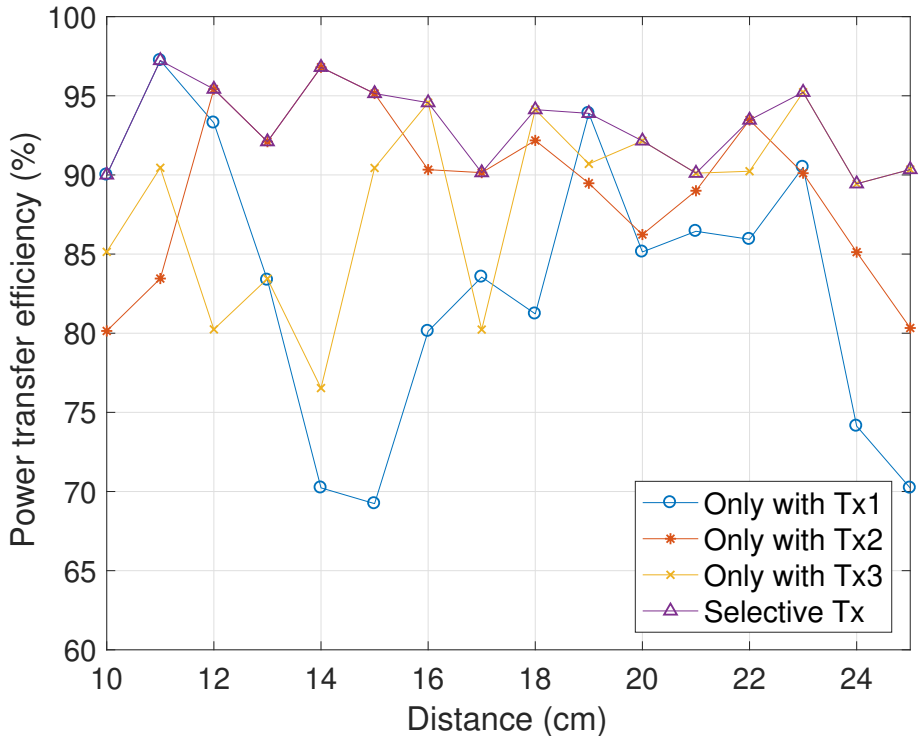

(b)

Figure 3.14: (a) The PTE without the selective Tx versus with the selective Tx in Case 1. (b) The PTE without the selective Tx versus with the selective Tx in Case 2.

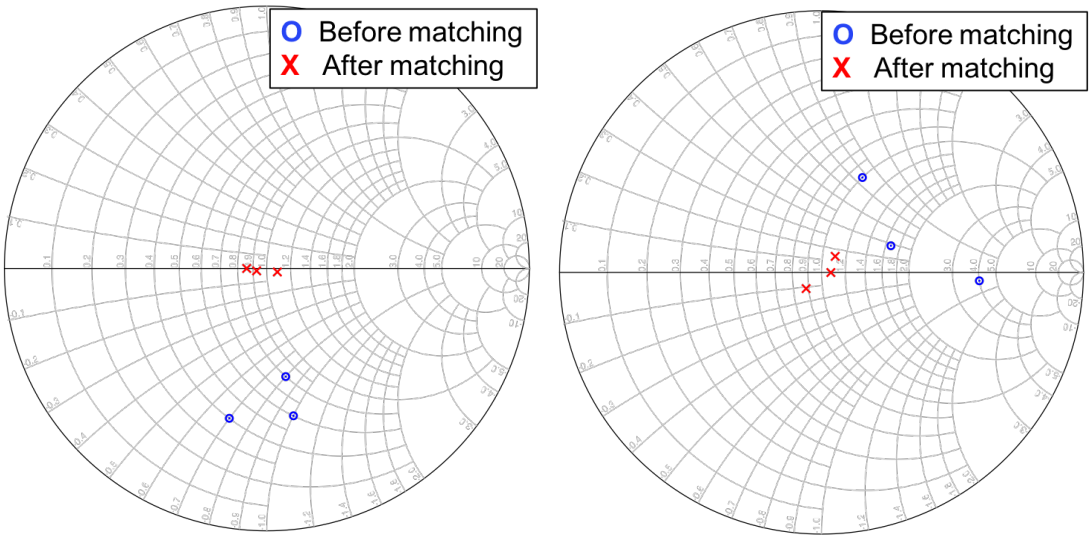

(a) (b)

Figure 3.15: Smith chart of the input impedance values of the system in angular misalignment at 10, 15, and 20 cm in: (a) -30° along ϕ angle. (b) +30° along ϕ angle.

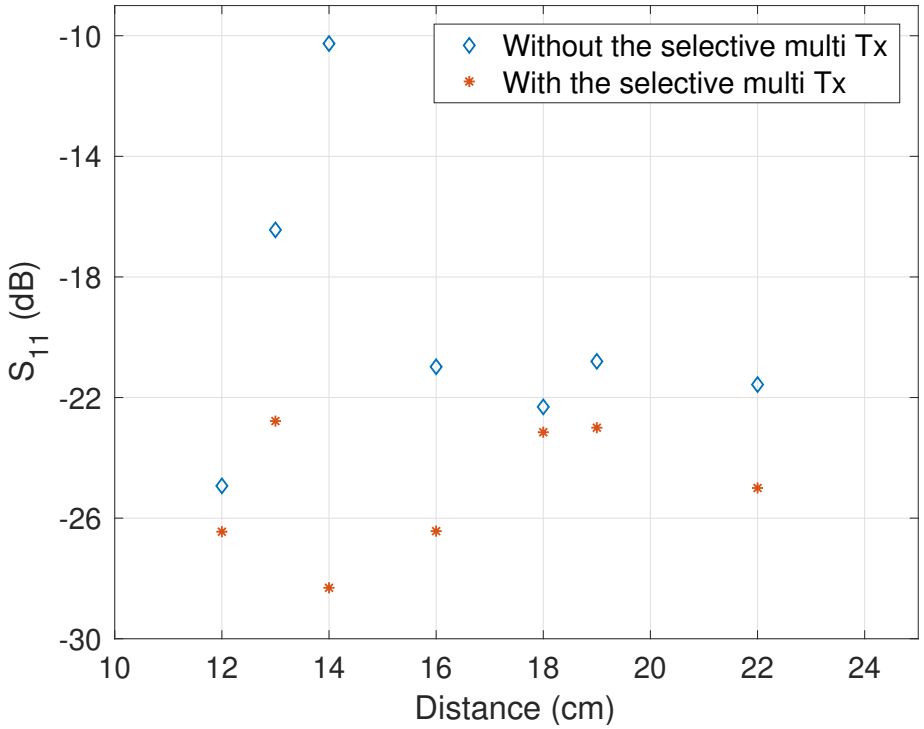

Figure 3.16: Transmitter selectivity.

Table 3.2: COMPARISON OF REPORTED RANGE-ADAPTIVE WPT SYSTEMS

	$\|S_{11}\|$ measurement for automatic matching	Tx-Rx structure	Type of matching circuit	Tuning method	Algorithm type/speed	Operation range(cm) over 80% of PTE
[23]	Directional coupler rectifier	Two resonators	L-type network in Tx	Relays (Switching capacitors)	Decent search with scaling,<1.5s	9-21
[24]	Rectifiers	Four resonators	π-type network in both Tx and Rx	Switching capacitors	Parasitic and conjugate match, -	10-22
[25]	Directional coupler rectifier	Four resonators	Shunt network in both Tx and Rx	Relays (Switching capacitors) varactors, multi-loop	Searching algorithm, <1.2s	10-40
[26]	Directional coupler RF detector IC	Two resonators	Cascading 6 L-type network in Tx	p-i-n diodes (Switching capacitors)	Genetic algorithm, <0.064s	10-16
[27]	Directional coupler RF detector IC	Four resonators	Γ-type network in Tx	Stepper motors for capacitors	Neural network, <0.063s	0-20
This work	**Directional coupler RF detector IC**	**Two resonators**	**Cascading 3 L-type network in Tx**	**Tunable capacitors p-i-n diodes multi-coil Tx**	**Neural network, <0.063s**	**10-25**

In an angular coil misalignment environment, the plane of the Tx coil is tilted to form an angle in the range -30° $< \phi <$ 30° at 10, 15, 20 cm as shown in Figure 3.13, and the system input impedance matching is improved as shown in the Smith chart in Figure 3.15. It can be easily seen that the matching results by the proposed method, even in an angular coil misalignment environment, are concentrated at the center of the Smith chart, which is close to target impedance 50 Ω.

In order to identify the performance of the range-adaptive impedance matching system and show the limitation of existing techniques, the comparison is shown in Table 3.2. Compared with the previous work utilizing GA [26], a significant improvement in the operation range while retaining high PTE was confirmed, with fewer circuit components that would otherwise have caused inevitable losses. Compared to the WPT systems configuration in [25] which employed the variable capacitances for the tunable matching circuit and selective multiloop to reduce the variation of the input impedance, the proposed WPT system utilizing the NN is more suitable for applications requiring speed which is the major limitation for real-time operation. Moreover, this work reveals the remarkable PTE enhancement over the entire separation distance range that can be achieved with the selective multi transmitters when compared with [27] in addition to the tunable matching circuit utilizing the NN algorithm.

3.5 Conclusion

This work describes the implementation of a machine learning strategy based on the NN for real-time range-adaptive automatic impedance matching of WPT applications [63]. In this chapter, range-adaptive impedance matching of WPT system utilizing NN algorithms was demonstrated. The implementation of the feedforward NN and pattern recognition

techniques for real-time range-adaptive automatic impedance matching of WPT applications can, not only, predict the capacitance value of the matching circuit under a specific environment, but can also select one of Tx coils which maximize Rx-Tx power transfer efficiency up to 95%. In addition, the proposed model is generalizable to contexts such as misalignment of Rx-Tx coils and a wide range of operation distances. The work reported here could greatly enhance the state-of-the-art real-time range-adaptive automatic impedance matching techniques in the WPT system.

CHAPTER 4

DESIGN OF A NOVEL WIRELESS POWER SYSTEM USING MACHINE LEARNING TECHNIQUES FOR DRONE APPLICATIONS

4.1 Introduction

In recent years, WPT has been increasingly required for many purposes from research and industrial communities, especially in applications of wireless charging systems for moving objects, such as automotive vehicles [64] and UAVs [65]. In particular, the global market for commercial applications of drone technologies is currently estimated at about $2billion, which will definitely balloon in the next decades. ML has become a major field of research in order to handle more and more complex detection problems [66]. With ML techniques, new state-of-the-art models can be developed by training a model instead of implementing an explicitly programmed feature detector. This work proposes a novel WPT platform that predicts the drone's behavior based on the flight data utilizing machine learning techniques incorporating Naive Bayes algorithms. The choice of Naive Bayes "classification" is due to its characteristics that are simple to implement and flexible enough to cover different types of measured data.

This chapter is organized as follows. Section 4.2 first demonstrates the measurement of the design and characterization of the proposed WPT system prototype, and Section 4.3 discusses the application of machine learning techniques based on the measurement data, and evaluates the WPT system performance.

4.2 WPT Platform Design and Characterization

The proposed WPT system consists of the transmitter array on the ground and a receiver on the drone as shown in Figure 4.1. A set of proof-of-concept measurements is performed for 2x2 to 4x4 transmitter arrays operating at 13.56 MHz. For both transmitter and receiver charging coils, we used an off-the-shelf planar coil from Wurth electronics with the specifications shown in Table 4.1 including the resonant frequency of 13 MHz, which can be adjusted to 13.56 MHz by connecting a tuning capacitor. N-channel single gate RF MOSFET transistors were employed for the switching of every individual transmitter coil and were controlled by a voltage source. The prototype is shown in Figure 4.2.

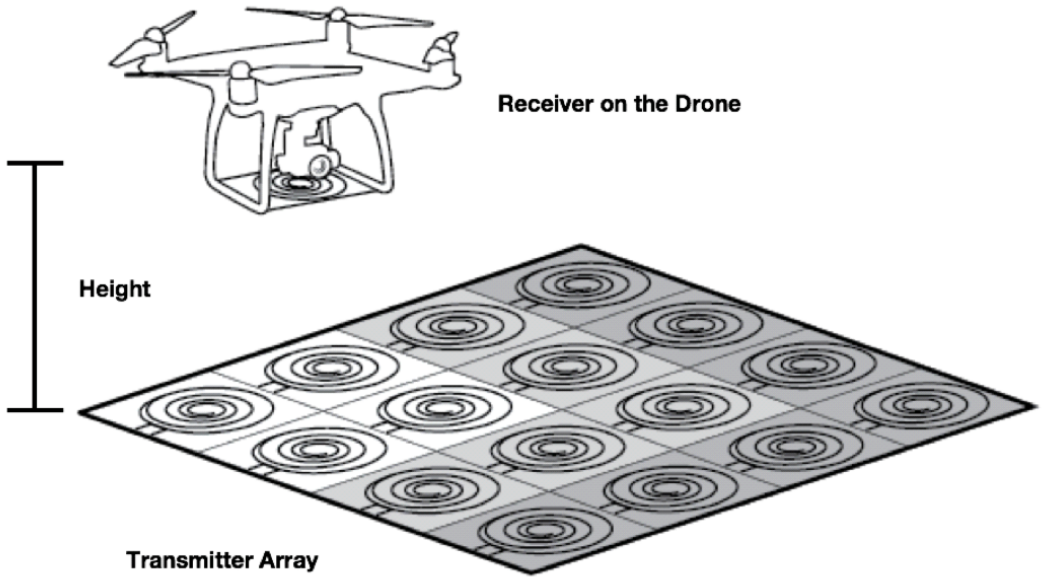

Figure 4.1: The proposed WPT system with an on-drone receiver and an on-the-ground transmitter array.

In order to accurately characterize the movement of the receiver coil on the drone, for a proof-of-concept topology, we utilized a 0.75 inch styrofoam 9-position (9-square) grid that

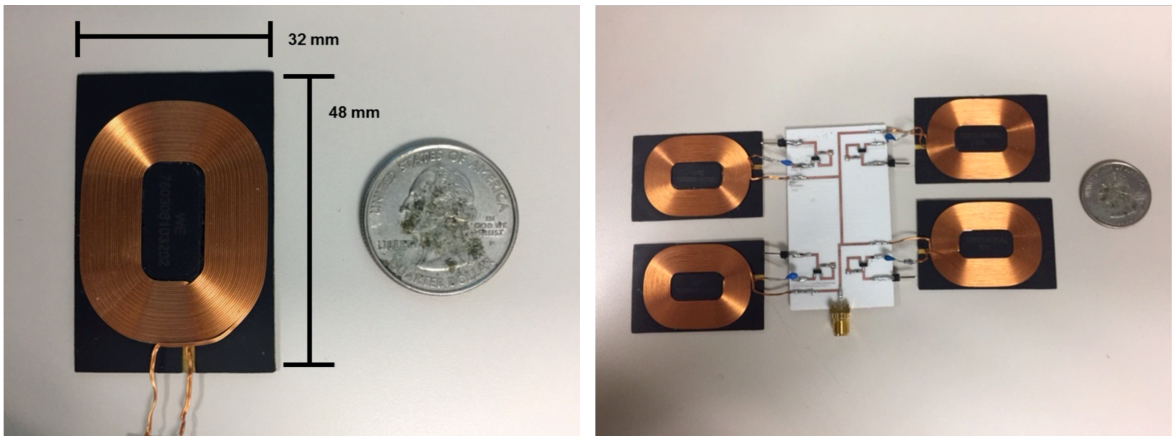

(a) (b)

Figure 4.2: (a) Off-the-shelf charging coil. (b) Prototype of 2x2 transmitter array.

Table 4.1: TRANSMITTING AND RECEIVING COIL SPECIFICATIONS

Parameters	Transmitter and Receiver
Inductance (μH)	12
Saturation Current (A)	6
Q-factor	33
DC resistance (Ω)	0.16
Self-resonant freq (MHz)	13

was placed on top of the transmitter array and then the S-parameters of the WPT topology were measured by placing the receiver coil on top of all 9 squares for all combinations of the 4 switches of the 2x2 transmitter array. The S-parameters of the topology were measured using a VNA, ZVA8 from Rohde&Schwarz, with a total 144 (4 switch, 9 positions) cases measured at the distances of 1inch, 1.25, 1.5 and 1.75 inch. The measurement setup is shown in Figure 4.3, the PTE is calculated as $|S21|$x100%, and the distribution of power transfer efficiency at each three distance are shown in Figure 4.4. From the preliminary measurements, the fabricated prototype exhibited relatively short operation range and low maximum power transfer efficiency. These are expected to be caused by the relatively small diameter of coils used for the array and low quality factor of the resonators. However, the

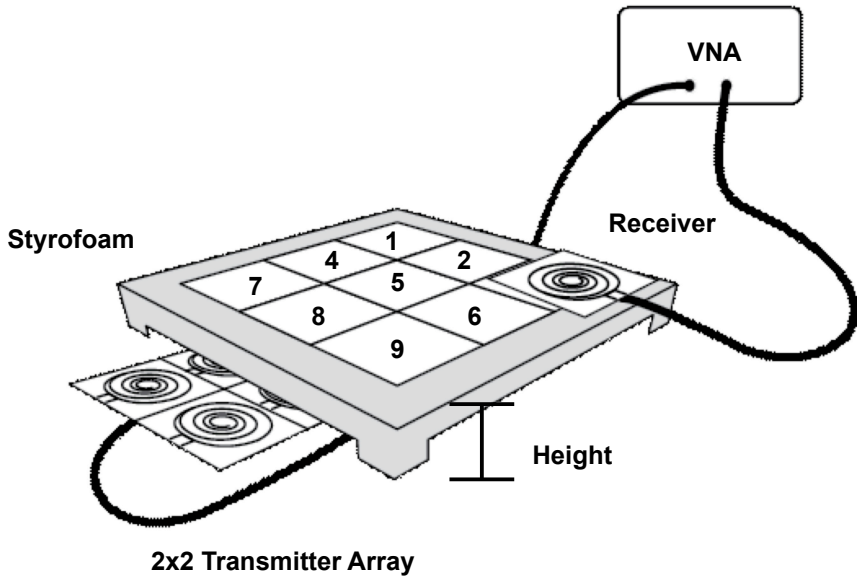

Figure 4.3: Illustration of the measurement setup.

system can be easily scaled to achieve higher operation range and the design of resonators can be improved to have a higher maximum power transfer efficiency.

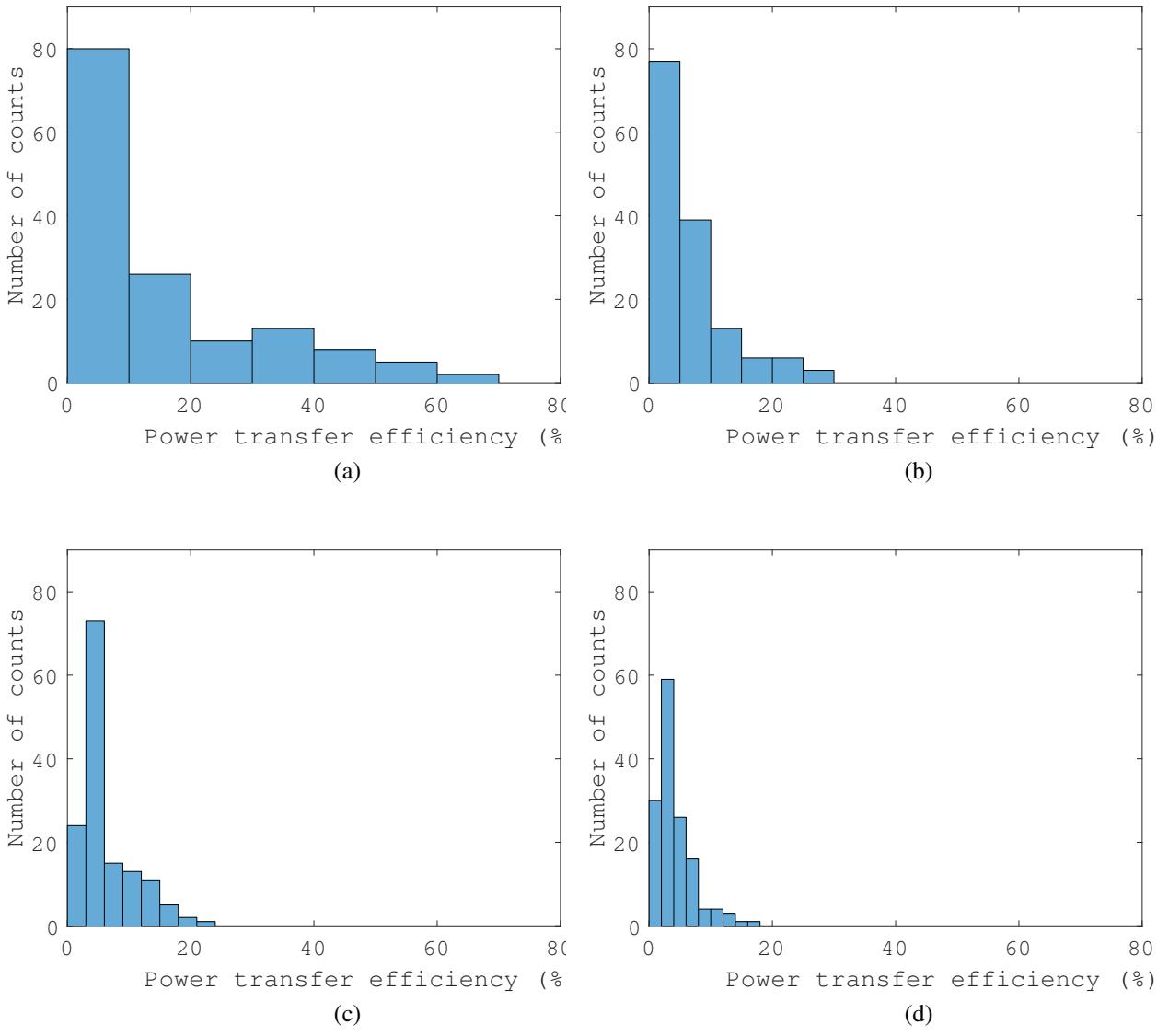

Figure 4.4: (a) Distribution of power transfer efficiency at 1 inch. (b) Distribution of power transfer efficiency at 1.25 inch. (c) Distribution of power transfer efficiency at 1.5 inch. (d) Distribution of power transfer efficiency at 1.75 inch.

4.3 Machine Learning Approach

Machine Learning has been successfully applied to numerous challenging problems and has drastically improved the efficiency of the designed systems and the design of machines. The learning is called "supervised" if instances are given with known labels corresponding to correct outputs [67]. The analysis of the trained data and produced an function of supervised learning algorithm can be used for mapping new instances.

4.3.1 Classification: Naive Bayes Algorithm

In this section, we evaluate the performance of the classification algorithm: Naive Bayes classifier. Classification is the supervised learning where a training set of correctly identified past observations is available [68], an approach that has been used in the past in fraud detection, market segmentation, and machine vision. The Naive Bayes algorithm is one of the classification algorithms that are simple and versatile and work very well in practice, as presented in chapter 1. Also, the Naive Bayes algorithm predicts the various sets of probabilities based on the condition values in a particular class. Bayes theorem provides a way of calculating the posterior probability, $P(C_k|x)$, from the prior probability of a class, $P(C_k)$, the likelihood which is the probability of predictor given class, $P(x|C_k)$, and the prior probability of predictor $P(x)$.

$$P(C_k|x) = \frac{P(C_k)P(x|C_k)}{P(x)} \tag{4.1}$$

$$P(x|C_k) = \prod_{i=1}^{n} P(x_i|C_k) \tag{4.2}$$

$P(x|C_k)$ be the conditional probability of seeing the evidence x if the hypothesis C_k is true. For any unseen test data, the method computes the posterior probability of that sample belonging to each class, then classifies the test data according to the largest posterior probability, as shown in equation (4.3).

$$y = \underset{k\in\{1,2,\ldots,K\}}{\arg\max}\ P(C_k)\prod_{i=1}^{n} P(x_i|C_k) \tag{4.3}$$

4.3.2 Performance Evaluation

In this work, the classification model is trained using Naive Bayes algorithms and then tested and validated using test data. For classification and prediction, the variables height, switching status of 4 transmitter coils, and each measured power transfer efficiency are assigned as "Predictor" in this learning. The number of receiver positions is assigned "Response" that will return a vector of the predicted class label for the predictor data, based on the trained Naive Bayes classification model. Consequently, the possible position of a moving receiver can be successfully predicted with a probability trend similar to actual measurement results. In Figure 4.5, the best and worst predictions are plotted by comparison with original data and predicted position at two operation distances. Not only at these four switching states, but at all switching states, the 3 positions having the highest achieved power transfer efficiency in descending order are selected and predicted. The prediction results show that the classification method provides great performance for predicting the receiver's position with obvious trends. As depicted in Figure 4.6, where the switching number means the state of 4 transmitter coils ($2^4 = 16$), the error rate varies from 0.09% up to 45% and the average value is 19.07%, 20.75%.

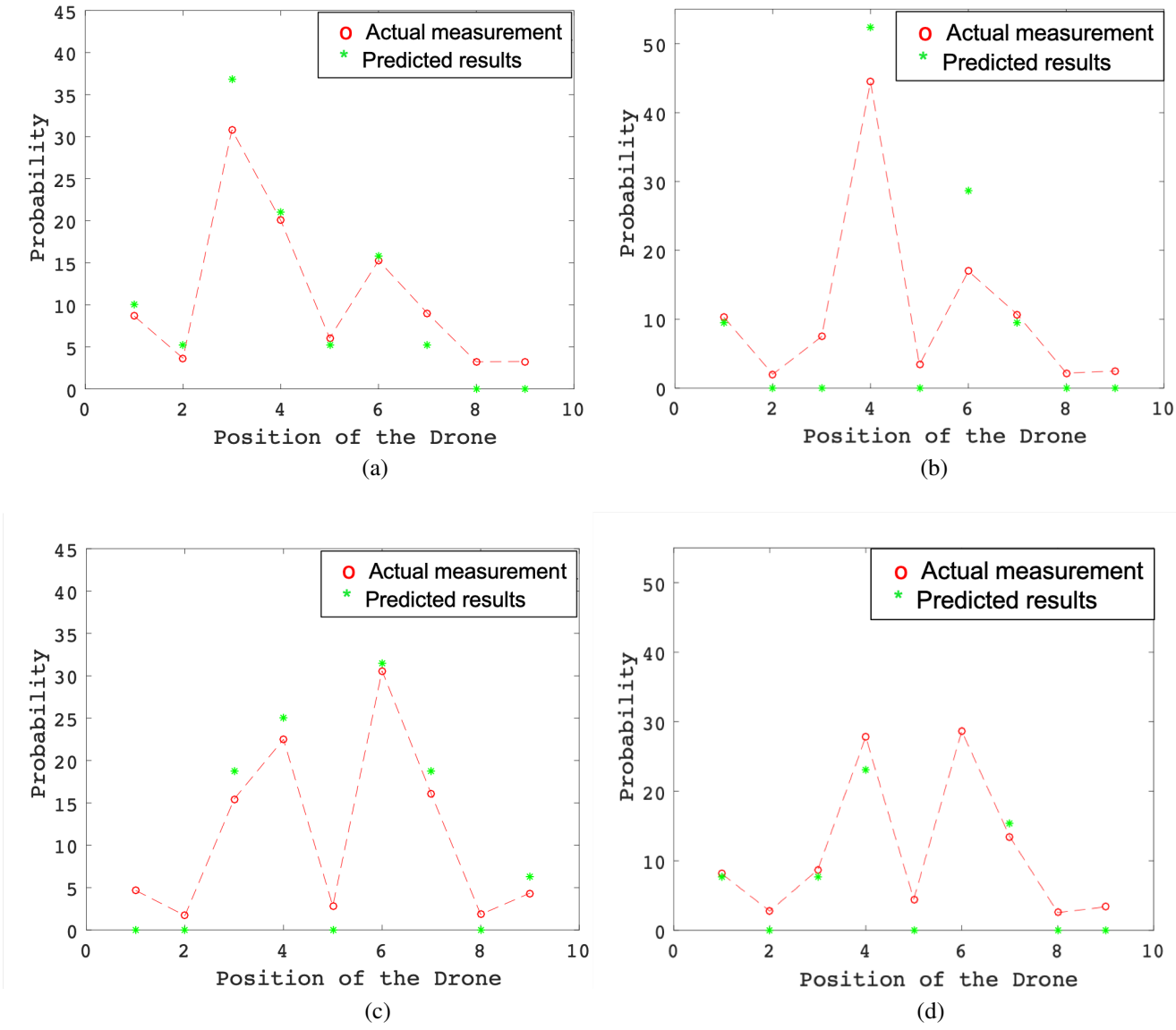

Figure 4.5: (a) Best prediction when the switching status "off-on-on-off" at 1 inch height (b) Worst prediction when the switching status "on-on-off-off" at 1 inch height (c) Best prediction when the switching status "off-on-off-off" at 1.25 inch height (d) Worst prediction when the switching status "on-on-on-on" at 1.25 inch height

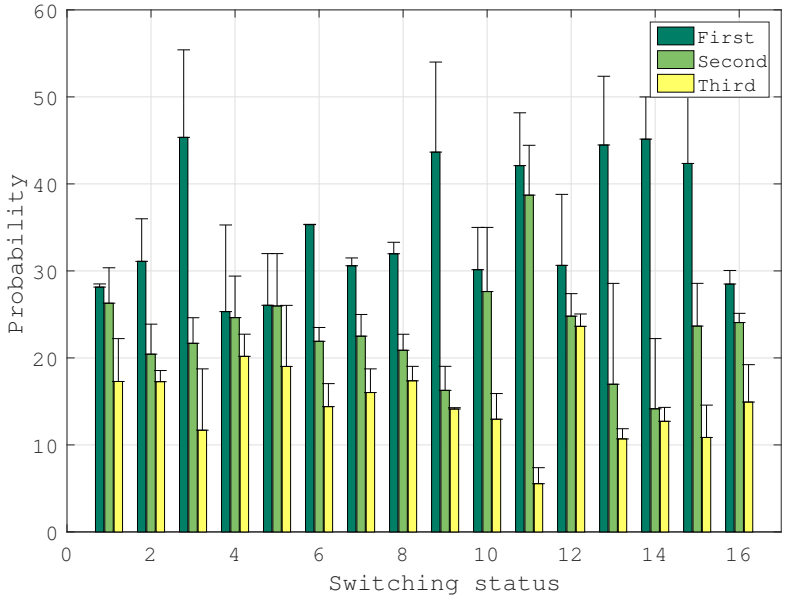

(a)

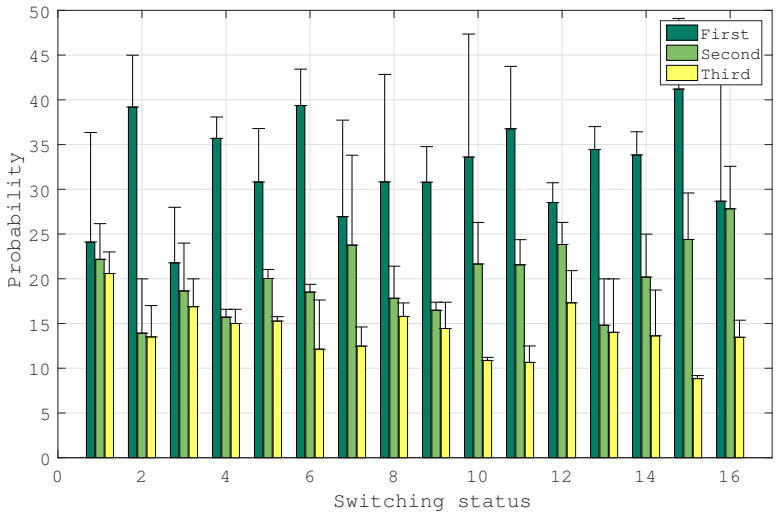

(b)

Figure 4.6: (a) Error bar at 1 inch height (b) Error bar at 1.25 inch height

4.4 Conclusion and Future work

In this chapter, the design of the WPT system combined with route prediction utilizing machine learning techniques for drone applications was proposed [69]. The position of

moving objects such as the drone can be predicted by introducing the Naive Bayes classification. The future works are 1) to expand the transmitter array and make automatic switching utilizing the Arduino Uno micro-controller unit by switching automatically 2) to extend the operation range and improve power transfer efficiency by a modified measurement environment. Moreover, integrating the designed system with a more practical environment for drone applications to implement a WPT platform.

CHAPTER 5

READ/IDENTIFICATION ENHANCEMENT OF CHIPLESS RFIDS USING MACHINE LEARNING TECHNIQUES

5.1 Introduction

Printable chipless RFIDs are a particularly appealing solution in contexts where cost is one of the most relevant constraints, as reported in [35]. However, these are very limited in reading range (a few meters) as a consequence of their linear operation and their sensitivity to interference. Cross-talk between reader antennas and environmental clutter interference can however be de-embedded but this approach cannot account for large contextual changes in the vicinity of the tag and reader. Also, the most commonly used tag detection techniques require the knowledge of signal processing methods or the careful and manual tuning of parameters including background subtraction, time gating, continuous wavelet transform, and match filtering in the reader side to process backscattered signal and extract the tag's data. Here, the author proposes an alternative approach that takes advantage of the immense pattern classification capabilities of modern machine learning techniques. For pattern classification, the SVM classification is used not only to make the reliable prediction but also reduce redundant information. Especially, this technique provides an excellent performance when dealing with high-dimensional input data by taking advantage of the fact that due to its generalization properties the performance of SVM does not depend on the dimensions of the space. The SVMs also obtained results comparable with those obtained by other classification methods utilizing machine learning strategy. Using these, it is possible to forego the aforementioned calibration approaches while retaining accurate reading

capabilities. In order to demonstrate this, a set of 2-bit chipless RFID tags with two T-shaped resonators encoding two distinct bits were first printed and their properties were described and measured. Then, a ML approach is devised, presented and implemented. Finally, the superiority of the machine learning approach is quantitatively demonstrated before a conclusion is drawn.

5.2 Experimental system overview

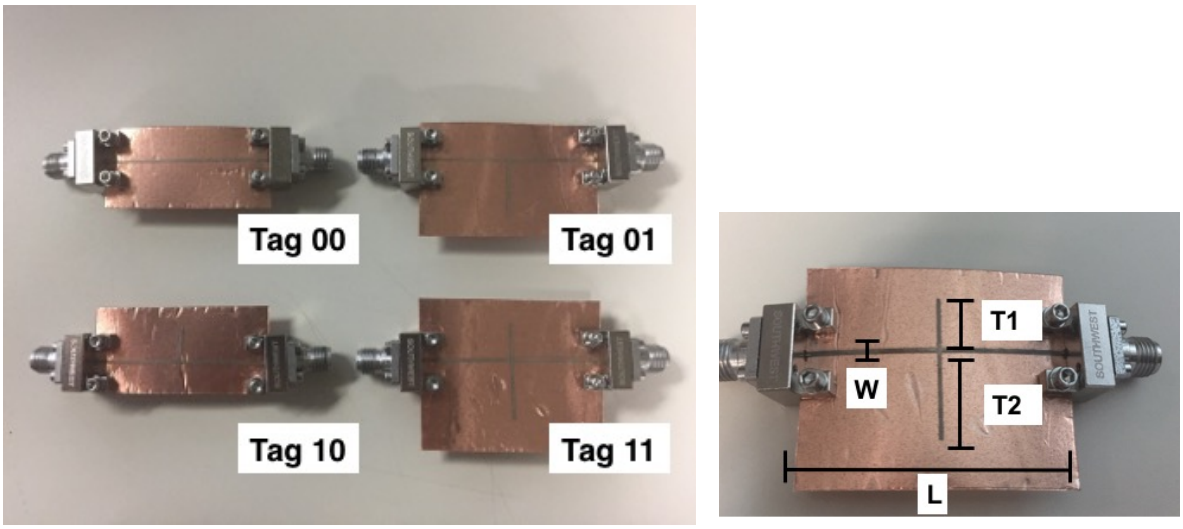

(a) (b)

Figure 5.1: (a) Inkjet printed chipless RFID tags. (b) Details showing the two T-shaped resonators encoding 2 bits.

5.2.1 Chipless RFID tag design and characterization

Four proof-of-concept chipless RFID topologies with two T-shaped resonant elements encoding all possible 2-bit combinations were inkjet-printed with silver nano particle on a PET substrate using a prototyping DMP2830 Dimatix inkjet printer. These topologies, shown in Figure 5.9, form the basis for the set of measured data that will then be used to train the ML algorithm. Each vertical microstrip line introduces a different stop-band

resonance at approximately 3.45 and 5.7 GHz that can be used as IDs representing logic '00', '01', '10' and '11'. The measured S_{21} values of all four tags are shown in Figure 5.2, and demonstrate the proper operation of the tags. The overall geometrical design for a T-shaped resonator is controlled by the key parameters summarized in Table 5.1 for each design of resonator.

Table 5.1: DESIGN PARAMETERS

	Length(L)	Width(W)	Tline 1(T1)	Tline 2(T2)
Tag '00'	40 mm	0.5 mm	None	None
Tag '01'	40 mm	0.5 mm	None	13 mm
Tag '10'	40 mm	0.5 mm	8 mm	None
Tag '11'	40 mm	0.5 mm	8 mm	13 mm

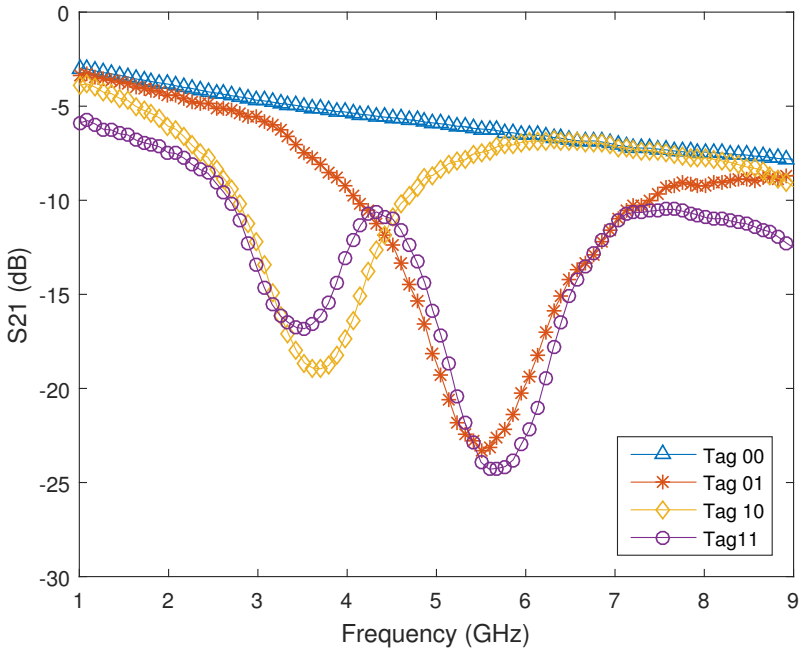

Figure 5.2: Wire measurement S_{21} results for the Tags '00','01', '10' and '11'.

Only the magnitude and phase information of the transmission coefficients (S_{21}), which serve as the channel transfer functions between the reader antennas at discrete frequencies,

were interested and used in the training.

5.2.2 Measurements

The proposed chipless RFID system consists of the transmitter reader/tag antennas, receiver reader/tag antennas and resonator tag attached to a styrofoam block in a realistic environment as shown in Figure 5.3. The Tx and Rx antennas were cross-polarized to enhance cross-talk isolation. The S-parameters of the system were measured using a vector network analyzer (VNA), ZVA8 from Rohde&Schwarz, with a total of 816 measurements varying in the range of interrogation distances 5 cm up to 50 cm (in step of 2 cm), in orientation (from -40° to +40° along phi(ϕ) angle, from -40° to +40° along theta(θ) angle) with consideration of the tag radiation pattern between reader and tag antennas as shown in Figure 5.4, and in the presence of clutter in the space separating the tag and the reader antennas (80 cases out of the 816). To emulate the clutter, a paper box was used with the size of (28 cm x 25 cm x 5.6 cm) and was always placed in the middle of the distance between the tag and the reader antennas. In other words, each tag underwent a total of 204 measurements varying the: 1) range of distances: 23, 2) orientation of angle: 160 from 5 cm to 50 cm in step of 5 cm, and 3) presence of clutter: 21 from 10 cm (start from 10 cm take the thickness of a paper box into account) to 50 cm in step of 2 cm. Measured S-parameters from 1 to 10GHz with 0.018 GHz interval (in total 500 points per measurement) were saved. The final size of dataset (816 x 500) for training was determined based on different aspects such as training speed, complexity of classification, and so on.

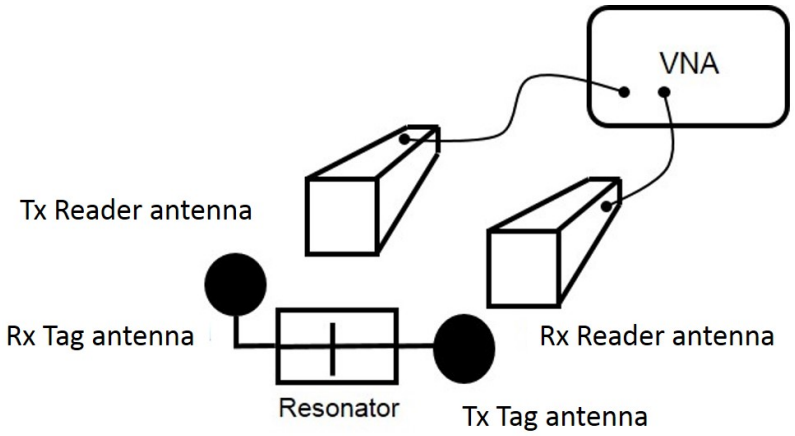

Figure 5.3: Illustration of the measurement setup of the chipless RFID system.

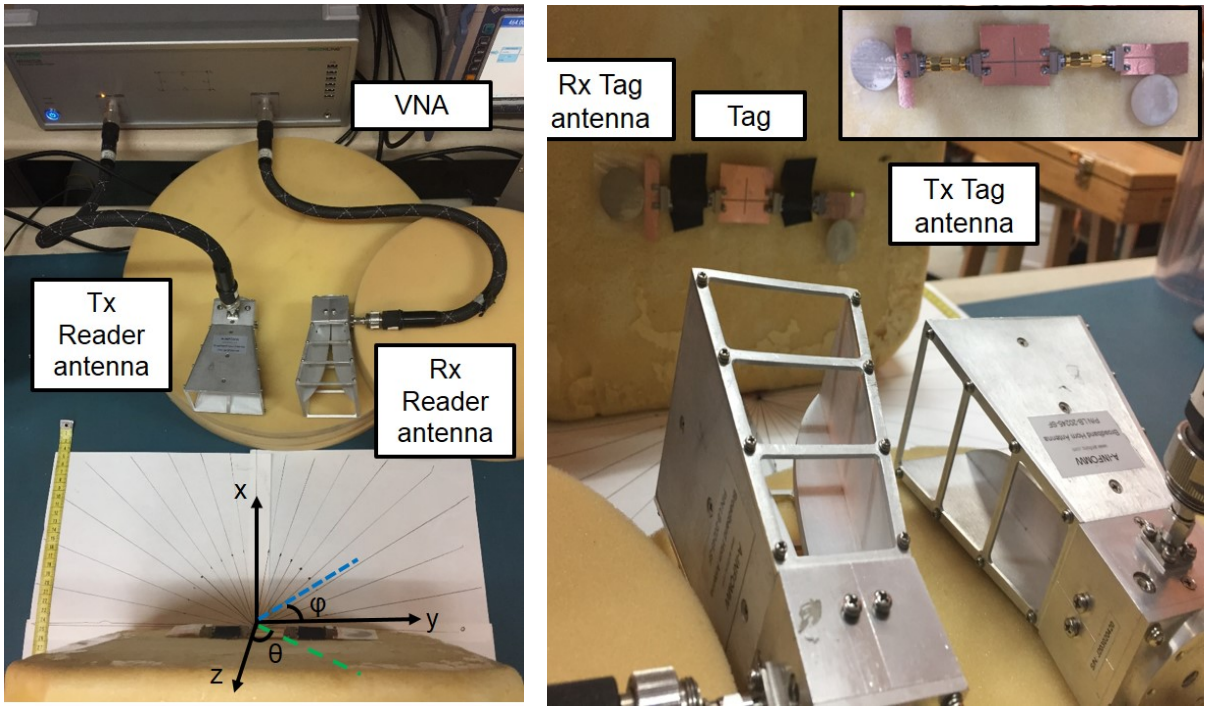

(a) (b)

Figure 5.4: (a) Measurement setup. (b) Measurement setup from reader side.

5.3 Machine Learning Approach

Machine Learning techniques have been widely applied to numerous challenging problems to make predictions or calculated suggestions based on large amounts of data. One algorithm of learning called "supervised" is useful in cases where instances are given with

a known dataset (the training dataset) corresponding to certain dataset in which prediction can later be made [48]. The trained model first is trained to produce a function of supervised learning algorithm and then uses a test dataset to validate the model. Based on the training dataset containing instances, classification could identify in which of a set of categories a new instance belongs. Several studies have been done for RFID-related applications utilizing machine learning techniques. The SVM classification has been used for personal healthcare application to collect and process multichannel data [70] and for learning-based self-localization to refine an estimation of a robot's location [71]. By applying numerous RFID applications, machine learning techniques provide tremendous benefits in terms of the predicted RFID tag detectability and the learning-based localization.

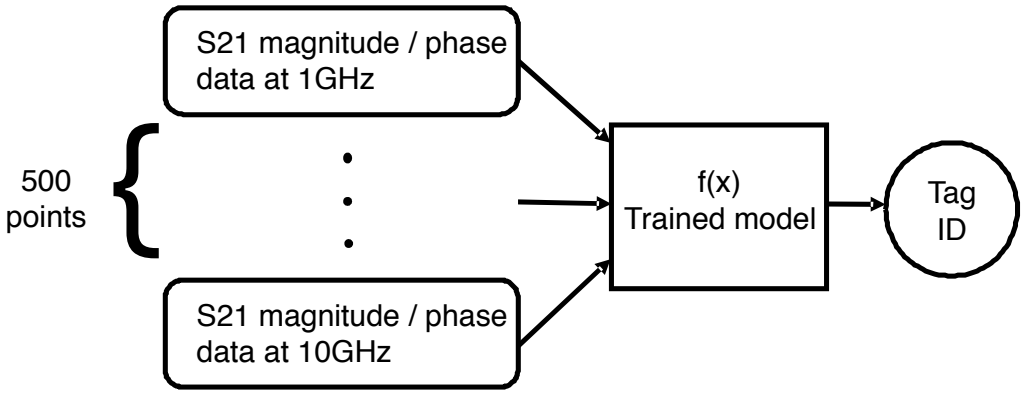

Figure 5.5: Proposed SVM tag ID detection.

In this application, we developed the SVM prediction model employing kernel tricks [72] with cross-validation to evaluate the accuracy. This SVM techniques were chosen because they have been applied to various classification problems such as development prediction models with high success [56]. The SVM essentially constructs a set of $(N-1)$ dimensional hyperplanes in N-dimensional space to separate data points into groups used for classification, as shown in Figure 2.4. When given a training dataset of n points of the form $\overrightarrow{x}_n, y_n$ where the y_i are either 1 or -1 indicating the class to where the point $\overrightarrow{x}_i$

belongs, any hyperplane can be written as the set of points $\overrightarrow{x}$ satisfying $\overrightarrow{w} \cdot \overrightarrow{x} - b = 0$ where $\overrightarrow{w}$ is the normal vector to the hyperplane and the parameter $b/\overrightarrow{||w||}$ determines the offset of the hyperplane. In this respect, the optimal separating hyperplane for which the margin is maximum is essential to place or locate unseen test points far away from the hyperplane or in the margin. By employing a polynomial kernel function (5.1) of a hyperplane, the points x in the d-dimensional feature space that are mapped into the hyperplane are defined by a relation such as $\sum_i a_i k(x_i, x)$ making it easy to compute the similarity in the original space.

$$k(x_i, x_j) = (x_i^T \cdot x_j + c)^d \tag{5.1}$$

The linear kernel function, if $c = 0$ (and $d = 1$), was finally used here. The final decision function given by (5.2) for new predictions which takes a dataset as input and gives a decision as output.

$$f(x) = sign \sum_{i}^{n} (a_i y_i) k(x_i, x_j) + b \tag{5.2}$$

The SVM classifiers are trained on the entire training set using the optimized parameters and evaluated for their performance on the test sets with kernel scale 5, which is the free parameter invariant and independent of the input dimension. Several types of the kernel functions with different kernel scale that were used in the training process are discussed in the next section. As mentioned in the previous section, the measured S_{21} parameters from 1 GHz to 10 GHz with 0.018 GHz interval (in total 500 points per measurement) were used as input data for the training process as shown in Figure 5.5. The targeted output of the algorithm was set as the meaningful parameter for practical chipless RFID use contexts:

Table 5.2: COMPARISON ACCURACY OF THE DIFFERENT TRAINED MODELS

	Decision trees	Boosted trees	k-nn	SVM
Magnitude data	59.6	73.7	67	**89.6**
Phase data	56	64.4	52.5	74
Magnitude & Phase data	60.7	76.7	55.7	86.2

namely, the IDs of the tags.

5.3.1 Performance evaluation

In order to detect the tag IDs, a training process using the proposed SVM classification with the measurement data previously described was implemented. The best SVM classifier achieved an accuracy of 98.3% when magnitude information of the measured transmission coefficient (S_{21}) were used for training process. It should be stressed that the reported reading success rates are those obtained for raw data, without any cross-talk or environmental-clutter removal calibrations. The total dataset was divided into 80% of the dataset to train the model and 20% of the dataset to test the performance of the trained model using k-fold cross validation which is a statistical method used to estimate the skill of of trained models. In other words, 163 datasets were taken out from the total dataset that had not been used for the training to demonstrate the robustness of the chipless RFID measurement approach, especially in challenging contexts such as those used here with large antenna crosstalk, close-by clutter and, thereby, difficult to extract tag IDs.

To identify the effect of the methods of different classification known as decision trees, boosted trees and k-nn with the SVM, each classification process was repeated and explored separately with different data sets composed with magnitude, phase and combined information of the measured transmission coefficient (S_{21}). Table 5.2 shows the result that the

Table 5.3: COMPARISON ACCURACY OF THE DIFFERENT KERNEL METHODS IN SVM

	Linear	Quadratic	Cubic	Gaussian
Kernel scale 1	89.6	90.5	90.2	56.8
Kernel scale 3	98	85.7	81.8	35.5
Kernel scale 5	**98.3**	88.1	83.7	24.2
Kernel scale 7	95.8	85.6	84.9	65.5

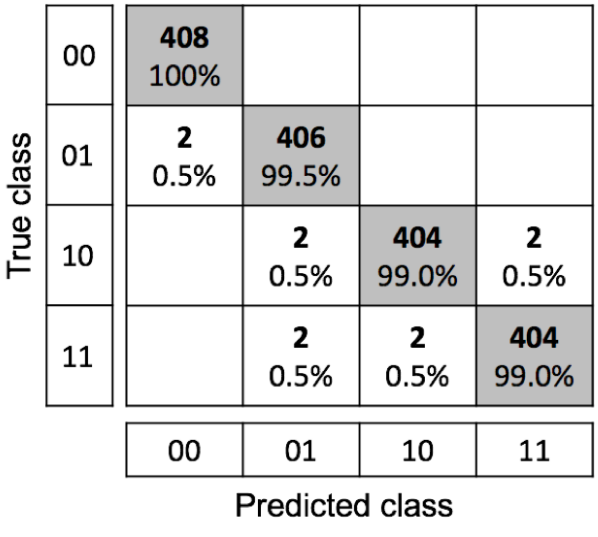

Figure 5.6: Confusion matrix for SVM I.

accuracy from training increases up to 89.6% even for the measurements at longer ranges when we use the SVM method with the dataset composed of magnitude data. Also, several kernel functions were explored including linear, quadratic, cubic and Gaussian using different kernel scale. Results obtained show that a linear kernel method based on kernel scale 5 outperforms the other methods for detecting tag's IDs with an accuracy of 98.3% as shown in Table 5.3. In this context, the algorithm demonstrates a remarkable performance for detecting tag's IDs. The confusion matrix using magnitude data for SVM with kernel scale 5, known as an error matrix in the field of machine learning classification is shown in Figure 5.6. The confusion matrix allows more detailed analysis and visualization of the performance of the trained model with SVM. It can be easily seen that the overall

classification is 98.3% and above 98% for all different tag IDs.

One can use different detection techniques [73]-[74] to identify chipless RFID tag IDs based on frequency-domain information, as reviewed in Table 5.4. To verify the fabricated chipless RFID tag IDs and show the limitations of existing techniques, the standard chipless RFID tag detection technique known as time-gating was used: its results are shown in Figure 5.7-(a) and (b), for distances of 10 cm and 30 cm. The process of time-gating follows the steps proposed in [73]. The frequency response of the tag '10' at a tag-reader distance at 10 cm—with a 3-4 ns time window—were readily obtained. However, at a distance 30 cm, the technique was unable to reliably detect the tags, as shown with the example of ID '10' in Figure 5.7-(b), then compared to the wire measurement S_{21} result for the tag '10'. In addition to the tag '10', the frequency response of the tag '01' at a tag-reader distance at 10 cm were obtained utilizing the time-gating method, as depicted in Figure 5.7-(c). Still, at a distance 30 cm in a different orientation +40° along theta(θ) angle, the technique was unable to detect the tags, as shown in Figure 5.7-(d).

Table 5.4: CHIPLESS RFID TAG DETECTION TECHNIQUES IN FREQUENCY DOMAIN II

	Tag type	Detection Technique	Freq (GHz)	Distance (cm)	Calibration	Anechoic chamber	Presence of object
[73]	Dual-band	Time-gating	2.5-5	10-25	background subtraction	Yes	No
[46]	Multi spiral	Amplitude & phase variation	2-2.5	5-40	use reference tag	Yes	No
[47]	Multi spiral	Signal space representation	2-3.5	up to 50	windowed signal	Yes	No
[75]	Alphabetic	Frequency scanning, pattern recognition	57-64	10-16	background subtraction	Not clear	No
[76]	Dual L-type dipole	Short-time Fourier transform	3-10	25	None	Inside & outside	No
[74]	Concentric rectangular loop	Time-gating / free-space antenna response subtraction	2-8	up to 50	None	No	No
This work	**T-shaped**	**SVM classification**	**0-10**	**5-50**	**None**	**No**	**Yes**

By contrast our SVM-based technique achieved better than 98% read rates at that distance even in different orientations, without requiring the knowledge of the distance and, therefore, of the time-gating delay. This work reveals the remarkable read/interrogate enhancement that can be achieved with this technique, without any required knowledge of the environment, and in practical conditions varying by operating distance and orientation.

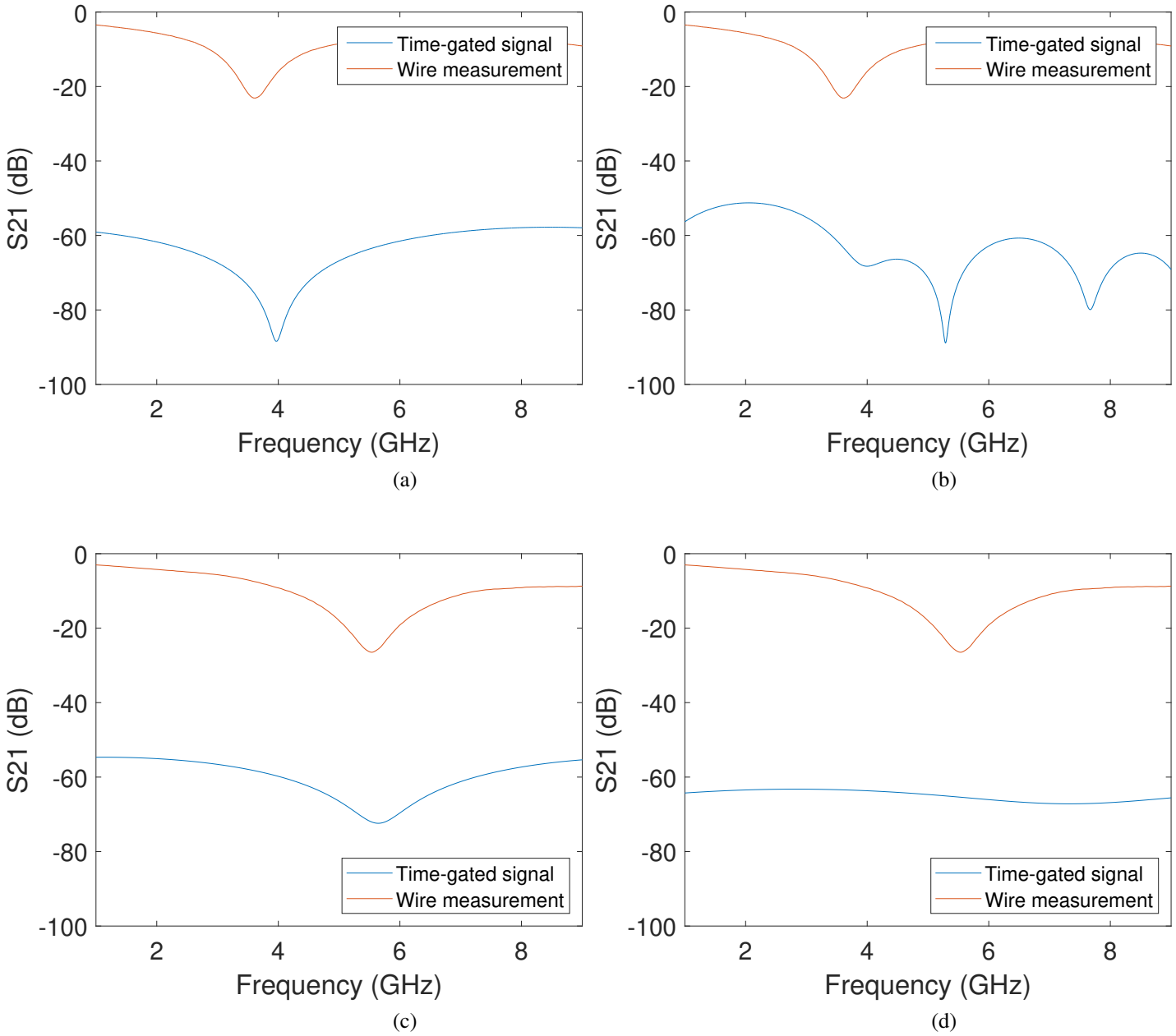

Figure 5.7: (a) Wire measured and time-gated signal for Tag '10' at distance 10 cm. (b) Wire measured and time-gated signal for Tag '10' at distance 30 cm. (c) Wire measured and time-gated signal for Tag '01' at distance 10 cm. (d) Wire measured and time-gated signal for Tag '01' at distance 30 cm in orientation +40° along theta(θ) angle.

5.4 Chipless RFID System for Robust Detection in Real-world Implementation

This work also describes a novel method based on a ML classification approach for highly accurate and robust identification of chipless RFID applications in a real environment. For this purpose, effective transponder reading is achieved not only for a wide variety of ranges and contexts but also for different commercial objects attached to the chipless RFID tag, while providing tag-ID detection accuracy of up to 98.5%. A vertically polarized UWB monopole transmitting tag antenna, four tags encoding the four 2-bit IDs, and a horizontally polarized UWB receiving tag antenna were also inkjet-printed onto a flexible low-cost PET substrate and interrogated without cross-talk or clutter interference de-embedding at ranges from 2 cm up to 50 cm, with different objects attached to the tag (non-conductive, aluminum can, and plastic bottle filled with water), and with and without the presence of scattering objects in the vicinity of the tags and reader. Several ML classification techniques are also explored, DT, k-NN, LDA, and SVM using the information of the measured transmission coefficients (S_{21}). Finally, an SVM method outperforms the other methods displaying reading accuracies 98.5%. A depolarizing chipless RFID tag [77] and a cross-polar orientation insensitive chipless RFID tag [78] were proposed to ease the detection of items in a real environment such as tagging the objects which have high reflective and high absorptive materials. However, these are limited in the reading range with the need of specialized tag design, and additional calibration/detection techniques such as background subtraction are required. Here, based on the above work [79], the first ML application for the enhanced accuracy with robust detection of chipless RFIDs regardless of the wide variety of the ranges and contexts, the tag's types, materials attached to the tag, is proposed.

5.4.1 Chipless RFID Tag design

The same chipless RFID tag topologies with two T-shaped resonant elements encoding all possible 2-bit combinations were used. To verify the detuning of the tag's resonator when changing the material to be attached, S_{21} values of all four tags were first simulated with a non-reflective object and highly reflective objects (aluminum can, plastic bottle filled with water). Simulation utilizing ANSYS HFSS shows that they get detuned when they are attached to highly reflective objects as shown in Figure 5.8. Without any required analysis of the effect of the microwave propagation on different material on the tag response, the superiority of the ML approach making detection of tag ID placed on conductive objects is quantitatively demonstrated. For practical implementations, a horizontally polarized UWB monopole receiving tag antenna, a T-shaped resonator, and a vertically polarized UWB transmitting tag antenna are fully printed and connector-free. The receiving and transmitting tag antennas are cross-polarized in order to minimize interference between the interrogation signal and the re-transmitted encoded signal containing the spectral signature. Photographs of the chipless RFID tag and antennas printed on PET substrate are shown in Figure 5.9.

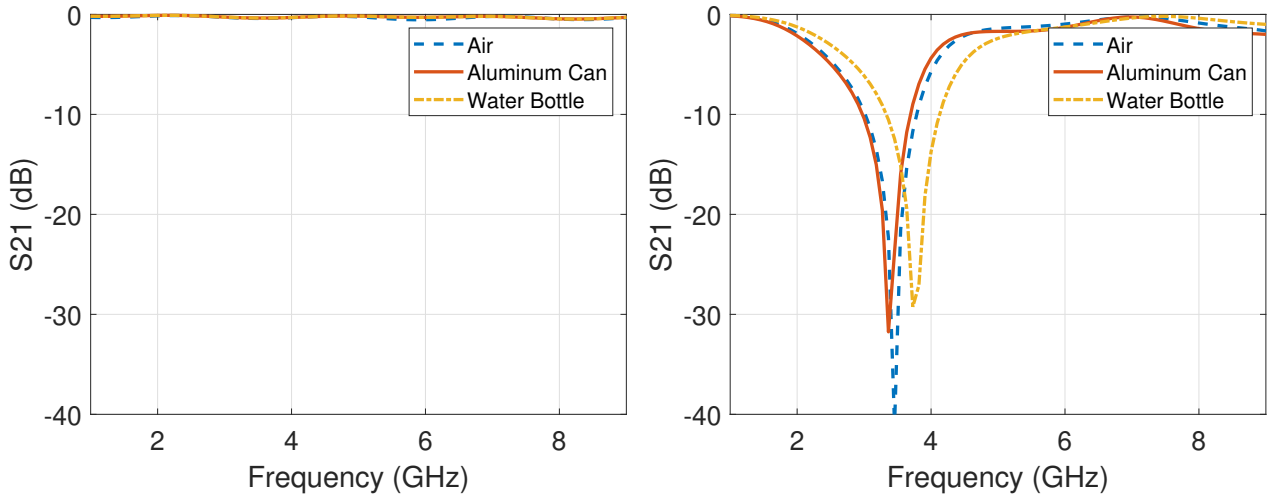

(a)

(b)

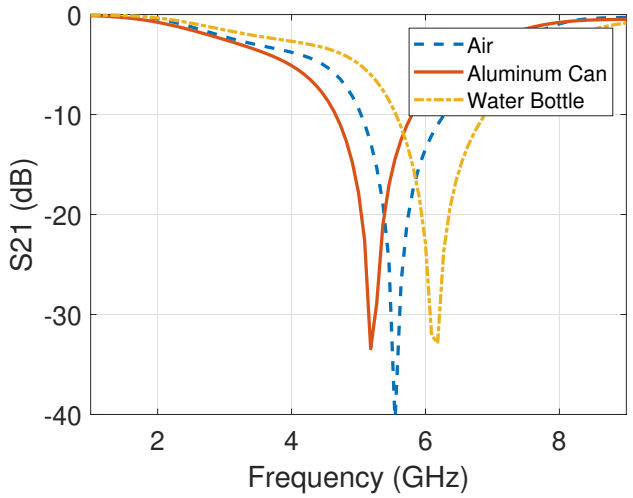

(c)

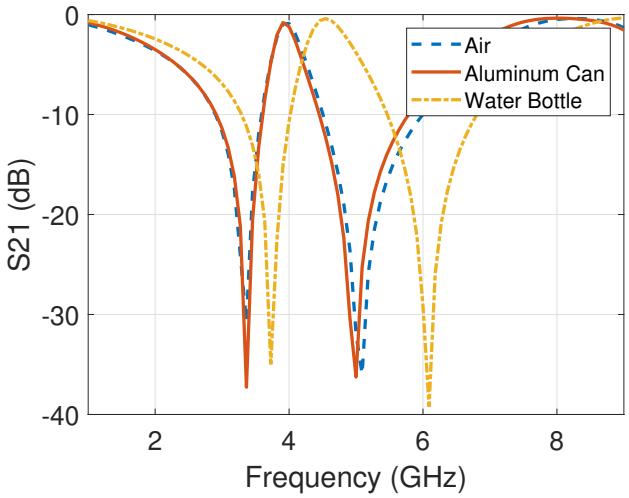

(d)

Figure 5.8: (a) Simulated S_{21} values of the tag '00' with respect to attached materials. (b) Simulated S_{21} values of the tag '10' with respect to attached materials. (c) Simulated S_{21} values of the tag '01' with respect to attached materials. (d) Simulated S_{21} values of the tag '11' with respect to attached materials.

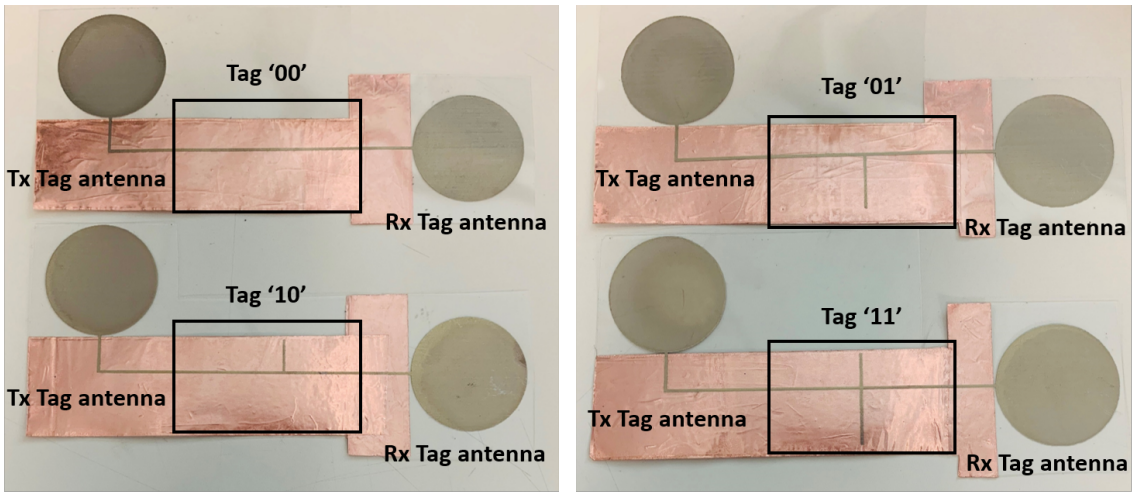

Figure 5.9: Inkjet printed chipless RFID tags and antennas.

5.4.2 Measurements and Data Collection with a variety of objects

Overall, the measurement setup is similar to that used in the previous section. The proposed chipless RFID system consists of the transmitter reader/tag antennas, receiver reader/tag antennas and resonator tag attached to different material objects (plastic box, aluminum can, and a plastic bottle filled with water) at a height of 8 cm from the ground, in a realistic environment as shown in Figure 5.10 and Figure 5.11. The Tx and Rx antennas were cross-polarized to enhance cross-talk isolation and placed on the sponge, a thickness of 4 cm. The S-parameters of the system were measured using a VNA, ZVA8 from Rohde&Schwarz, with a total of 612 measurements varying over a range of interrogation distances from 2 cm to 50 cm (in steps of 3 cm), with the tag placed are different objects. We also considered the radiation pattern between the reader and tag antennas, and the presence of clutter in the space separating the tag and the reader antennas. To emulate the clutter, a paper sheet and a copper sheet were used of size 18 cm x 20 cm and was always placed in the middle of the distance between the tag and the reader antennas as shown in Figure 5.12-(b),(c).

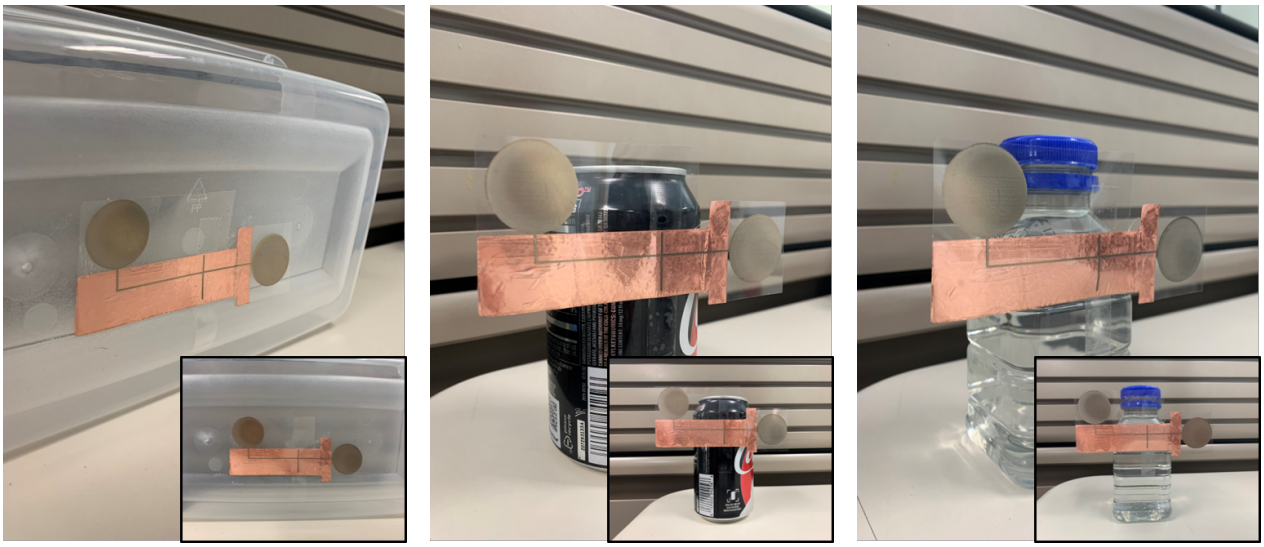

(a) (b) (c)

Figure 5.10: (a) Tag attached to the plastic box. (b) Tag attached to the aluminum can. (c) Tag attached to the plastic bottle filled with water.

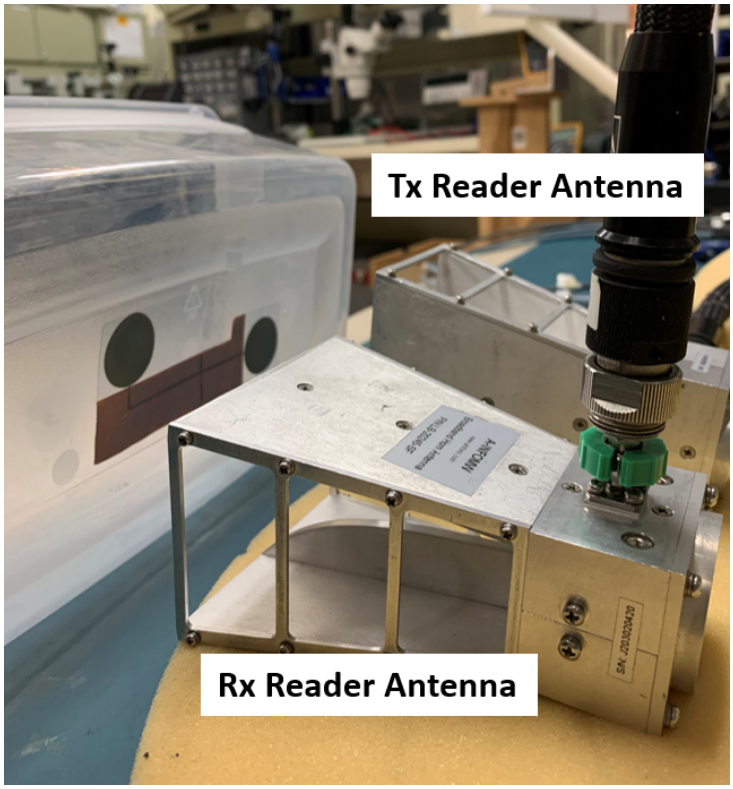

Figure 5.11: Measurement setup from reader side.

Table 5.5: SPECIFIED COMPOSITION OF THE DATASET PER TAG

	No clutter	Paper sheet	Copper sheet
Plastic box	17	17	17
Aluminum can	17	17	17
Bottle filled with water	17	17	17
153	51	51	51

In other words, each tag underwent a total of 153 measurements varying the: 1) range of distances, 2) object materials, and 3) presence of clutter, and detailed measurement setup specified in Table 5.5. Measured S-parameters from 1 to 10 GHz with 0.018 GHz interval (in total 500 points per measurement) were saved. The final size of the dataset (612 x 500) was determined for training based on different aspects such as training speed, complexity of classification, and so on. Only the S_{21}, which serves as the channel transfer function between the reader antennas at discrete frequencies, were used in the training. To acquire the 612 measurement dataset faster, the MATLAB Instrument Control Toolbox is used to communicate with a VNA directly for collecting and analyzing data, visualizing the results, and automating test without having to save and import it into MATLAB at a later time.

5.4.3 Performance Characterization of tag detection

The cubic kernel function, if $c = 0$ (and $d = 3$), outperforms the other classification techniques, and several types of the kernel functions that were used in the training process are explored in this section.

In order to detect the tag IDs, a training process using the several classification algorithms with the measurement data previously described was implemented. Each classification process was repeated and explored separately with different data sets composed with magnitude, phase, real part, imaginary part, and combined information of the measured S_{21}.

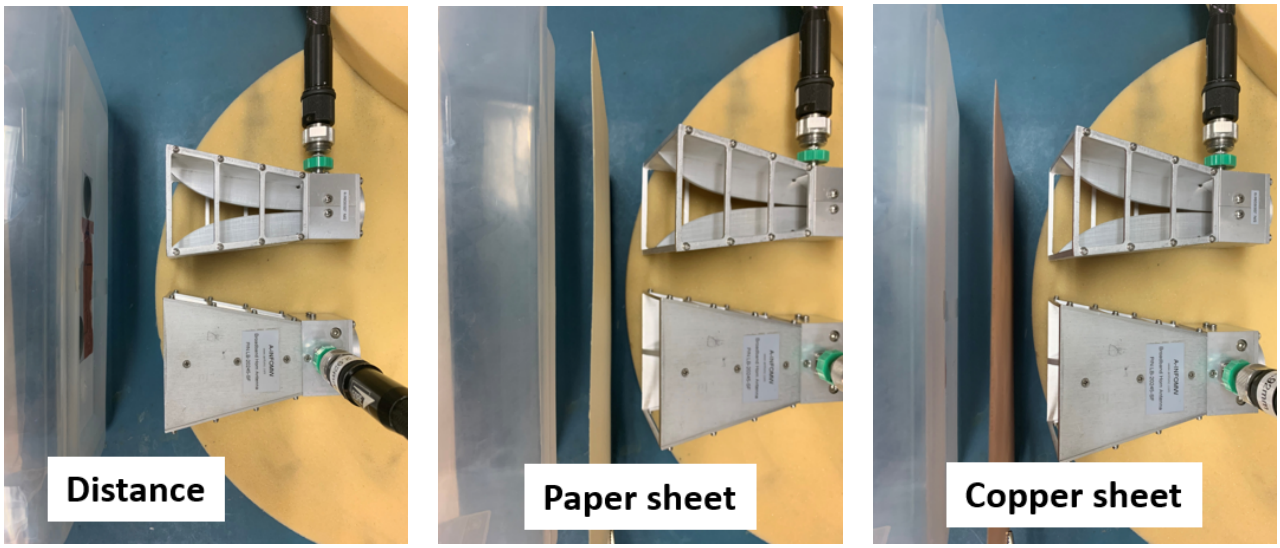

(a) (b) (c)

Figure 5.12: (a) No object between the tag and the reader antennas. (b) Paper sheet between the tag and the reader antennas. (c) Copper sheet between the tag and the reader antennas.

Table 5.6: COMPARISON ACCURACY OF THE DIFFERENT TRAINED MODELS

	Decision Trees	k-NN	LDA	SVM
Magnitude	43.5	52.3	70.3	70.6
Real	28.9	38.9	58.8	42.2
Magnitude & Phase	86.9	97.2	**98.2**	**98.5**
Real & Imaginary	79.9	96.6	97.2	90.3

In such way, the accuracy of detection increases due to the wealth of information available to the algorithm from the multidimensional dataset constructed from the concatenation of the combined information. The investigations were carried out using multidimensional information generated from various possible combinations of all or subsets of magnitude, phase, real, and imaginary information of S_{21} which form the hybrid features. Results, presented in Table 5.6, based on these combined features show indeed a substantial improvement in the algorithm prediction resulting in significant enhancement in tag ID detection. Table 5.6 shows that the LDA classifier achieved an accuracy of 98.2% when magnitude and phase information of the measured S_{21} were used for training process. Moreover, k-

Table 5.7: ACCURACY WITHOUT SPECIFIED COMPOSITION OF THE DATASET

	No object		Paper Sheet		Copper Sheet	
	SVM	LDA	SVM	LDA	SVM	LDA
Plastic box	67.1	69.5	67.6	68.9	74.8	79.4
Aluminum can	69.1	68.4	70.6	68.6	75.2	76.1
Bottle filled with water	67.6	69.9	68.9	67.8	75.7	75.2
Average Error rate	31.4		31.27		**23.93**	

NN classifier also exhibits high accuracy of reading success rates above 96% for raw data, without any cross-talk or environmental-clutter removal calibrations. For SVM classification, several kernel functions are explored including linear, quadratic, cubic and Gaussian functions. Results obtained show that a cubic kernel method outperforms the other methods for detecting tag's IDs with an accuracy of 98.5%, as also shown in Table 5.6. In this context, the algorithm demonstrates a remarkable performance for detecting tag's IDs comparable with those obtained by other classification methods. The confusion matrix using magnitude and phase data for cubic SVM, known as an error matrix in the field of machine learning classification, is shown in Figure 5.13. That matrix allows more detailed analysis and visualization of the performance of the trained model with SVM. It can be easily seen that the overall classification is 98.5% and the individual classification is above 97% for all different tag IDs.

5.4.4 Detection Results in Different Context

One of the fundamental motivations for this research was to create a practical chipless RFID tag reading system, which can ease the detection of items in a real environment such as not only tagging the objects which have high reflective and high absorptive materials

but the presence of scattering objects in the vicinity of the tags and reader. To verify the effect of the material and the presence of objects, extracted dataset of specific composition (17*4=68) from the whole dataset has not been used for the training. In other words, 68 datasets were taken out from the total dataset that have not been used for the training to demonstrate the effect of the specific dataset. As Table 5.7 clearly shows that the accuracy changes with the material behind the tag and the presence of objects, the accuracy can improve tag ID detection, especially without the data of challenging contexts such as the presence of copper sheet between the reader and tag antennas. After training with 544 measured data points while leaving 68 others with the proposed SVM and LDA classification, the trained model displayed the lowest error rate of around 23.93%, as shown in Table 5.7, for measurement data sets with a copper sheet that were not included in the training. It can be said that dataset composed of measurement with copper sheet has more impact on classification capability than other factors. Although the tag ID detection accuracy decreased up to 12% with the highly reflective object between the reader and tag antennas, over 97% of accuracy achieved utilizing combined features discussed in the part (5.4.3), suppressing the effect of the environment and highly reflective objects.

To further understand the ability of the trained model to read chipless RFID tag IDs according to the distance at 5-50 cm, the detection and actual ID values of each different test sets were analyzed. Each test sets composed of 12 measurement configurations at constant ranges of 5-50 cm in step of 3 cm, but with changing attached materials or types of objects were taken out from the total dataset. Since the amount of original data used for the training was relatively independent between each measurement sets, extracted test sets from the measured data are essential to verify the prediction capability. Another reason to create the test set from measured data that has not been used for the training before in this application

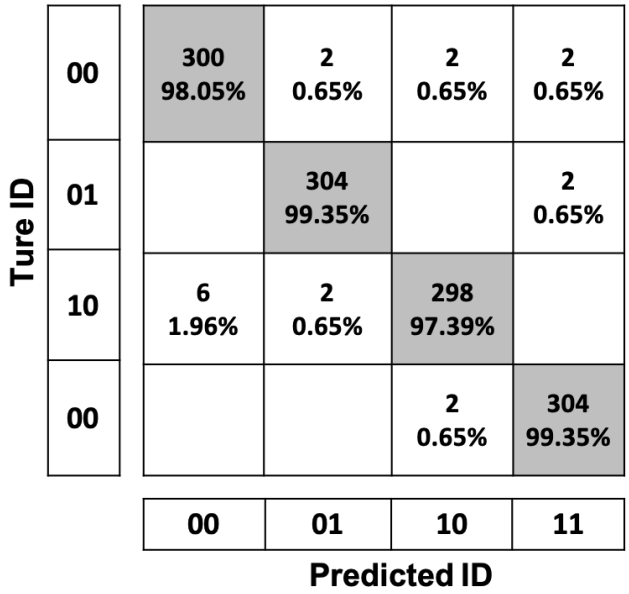

Figure 5.13: Confusion matrix for SVM II.

is to demonstrate the robustness of the chipless RFID measurement approach, especially in challenging contexts such as that used here with large antenna crosstalk, close-by clutter and, thereby, difficult to extract tag IDs. After training with 1200 (600 of magnitude data and 600 of phase data) measured datasets while leaving 24 (12 of magnitude data and 12 of phase data) others at each distance for testing with the proposed SVM classification, the trained model displayed an accuracy above 90% during self-testing within 40 cm except for the case of the datasets with the copper sheet object close-by, as shown in Figure 5.14, for datasets that were not included in the training. For example, 100% of accuracy in Figure 5.14 is calculated where the trained model correctly detects 24 tag's IDs among 24 cases of the test dataset. This work also reveals the remarkable read/interrogate enhancement that can be achieved with this technique, without any required knowledge of the environment, and in dynamic cluttered environments without the need for additional calibration.

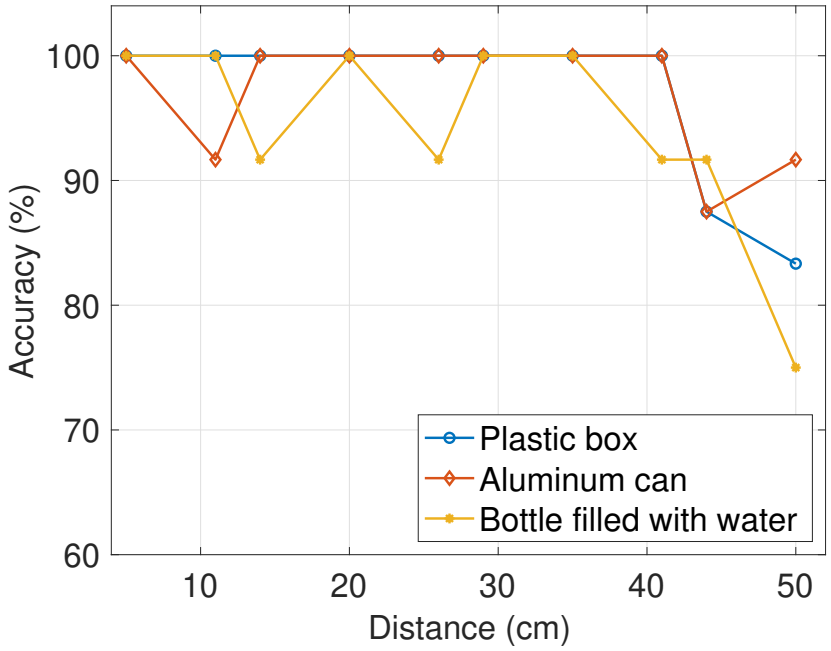

(a)

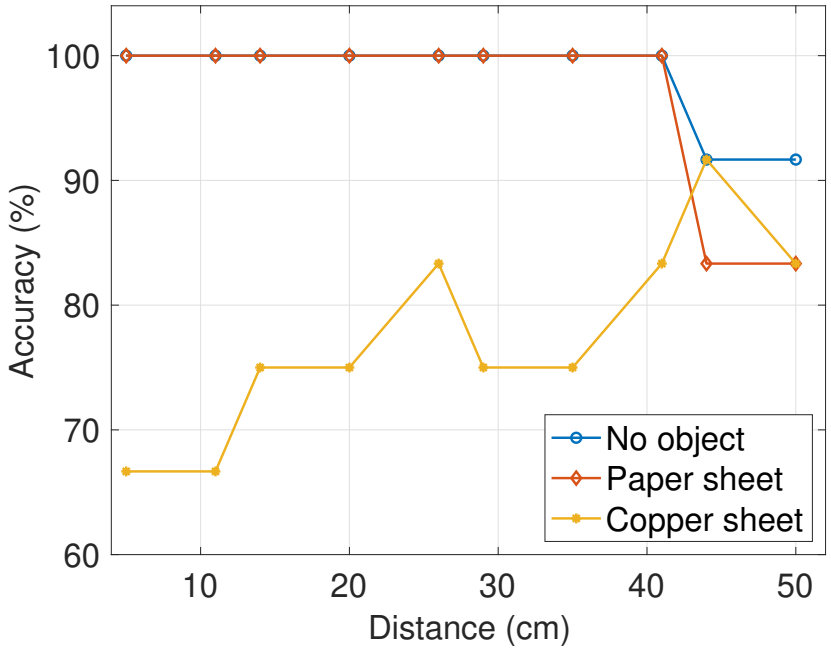

(b)

Figure 5.14: (a) Detection accuracy with different material attached to the tag at different distances. (b) Detection accuracy with different object between reader and tag antennas at different distances.

5.5 Conclusion

In this chapter, the implementation of a specific machine learning technique, SVM classification, to detect the chipless RFID tag IDs was demonstrated. Besides, high reading accuracies (above 97%) were achieved without environmental calibration, even in the cases of different orientations and with the presence of objects between the reader and tag antennas. The proposed detection model is very scalable and generalizable to context for a large number of tags, with a much higher number than the 2 bits used here, and with additional influence factors.

The polarization dependence is one of the challenging issues of the chipless RFID system, especially when placed different material objects such as highly reflective or absorptive. In this work, the first application of such concepts for the enhanced accuracy detection of chipless RFIDs is proposed for robust reading ability in the real environment and regardless the material of objects (highly reflective and absorptive) attached to the tag without the additional processes such as background subtraction technique, calibration for the specific material, and use of any featured tag.

Moreover, this approach effectively achieves the improvement in terms of reading range, robustness to orientation change and environmental clutter. While most of the TDR-based tags were a technical success in above mentioned, SAW RFID tags have limitation because SAW tags could only implement a limited set of unique ID numbers. By exploration of tag's performance with the proposed method utilizing ML classification for denser bit implementations as the topic of future efforts, this research opens up a large number of applications in which it is fundamental to support long read range, high data capacity and high resistance to environmental conditions.

CHAPTER 6

CONTRIBUTION AND CONCLUSION

6.1 Conclusion

In this thesis, the research on ML applications of wireless power transfer and identification technology was examined. The primary goal of this research was to develop the implementation of a ML strategy based on 1) the NNs for real-time range-adaptive automatic impedance matching of WPT applications, 2) the Naive Bayes classifier for the prediction of the drone's position, thus enhancing the WPT efficiency, and 3) the SVM classification strategy for read/interrogation enhancement in chipless RFID applications.

Chapter 2 provides the preliminary background of ML classification techniques by addressing their processes and relative advantages in detail.

Chapter 3 demonstrates ML applications for the WPT systems, including the automatic real-time range-adaptive impedance matching network. This approach for the effective prediction of the optimal parameters of the tunable matching network and selection range-adaptive transmitter coils (Tx) is introduced in this dissertation aiming to achieve an effective automatic impedance matching over a wide range of relative distances. We propose a WPT system consisting of a tunable matching circuit and 3 Tx coils which have different radius controlled by trained NN models. Also, a prototype of the entire real-time range-adaptive automatic impedance matching system is built and characterized. Finally, the proposed approach achieves a PTE around 90% for ranges within 10 to 25 cm, is reported.

Chapter 4 presents the design and performance of ML application for the WPT systems in UAV localization utilizing drones with machine learning techniques. Research on drones

is currently a fast-growing field with great potential in many ubiquitous applications. The wireless power transfer system with the fixed operation frequency at 13.56 MHz is applied to a 1-coil receiver on the drone, with an array of transmitter coils on the ground. This work presents an approach where the data is considered "classified" using machine learning techniques, which allows the accurate prediction of the drone's position, thus enhancing the wireless power transfer efficiency.

Chapter 5 demonstrates ML applications for the chipless RFID system in read/interrogation enhancement. A novel ML-based approach for classification and of detection tag IDs has been presented which can perform effective transponder readings for a wide variety of ranges and contexts while providing tag-ID detection accuracy of up to 98.3%. Four tags encoding the four 2-bit IDs were inkjet-printed onto a flexible low-cost PET substrates and interrogated without cross-talk or clutter interference de-embedding at ranges up to 50 cm, with different orientations in the vicinity of the tags and reader. A SVM algorithm was then trained using 816 measurements and its accuracy was tested and characterized as a function of the included training data. Finally, the excellent performance of the approach, displaying reading accuracies ranging from 89.6% to 98.3%, is reported. Also, a vertically polarized UWB monopole transmitting tag antenna, four tags encoding the four 2-bit IDs, and a horizontally polarized UWB receiving tag antenna were inkjet-printed onto a PET substrates and interrogated without cross-talk or clutter interference de-embedding at ranges from 2 cm up to 50 cm, with different objects attached to the tag (non-conductive, aluminum can, and a plastic bottle filled with water), and with and without the presence of scattering objects (paper sheet and copper sheet) in the vicinity of the tags and reader. Finally, a SVM method outperforms the other methods displaying reading accuracies 98.5%.

These efforts set a precedent, opening the door to a rich and wide area of research

for the implementation of ML methods for the enhancement of WPT and chipless RFID applications.

6.2 Publications

6.2.1 Refereed Journals

1. S. Jeong, T. Lin and M. M. Tentzeris, "A Real-Time Range-Adaptive Impedance Matching Utilizing a Machine Learning Strategy Based on Neural Networks for Wireless Power Transfer Systems," in IEEE Transactions on Microwave Theory and Techniques, vol. 67, no. 12, pp. 5340-5347, Dec. 2019.

2. S. Jeong, J. G. D. Hester, W. Su and M. M. Tentzeris, "Read/Interrogation Enhancement of Chipless RFIDs Using Machine Learning Techniques," in IEEE Antennas and Wireless Propagation Letters, vol. 18, no. 11, pp. 2272-2276, Nov. 2019.

3. S. Jeong, J. G. D. Hester, R. Bahr and M. M. Tentzeris, "A Machine Learning Approach-based Chipless RFID System for Robust Detection in Real-world Implementations," in IEEE Antennas and Wireless Propagation Letters. (Submitted)

4. J. Bito, S. Jeong and M. M. Tentzeris, "A Novel Heuristic Passive and Active Matching Circuit Design Method for Wireless Power Transfer to Moving Objects," in IEEE Transactions on Microwave Theory and Techniques, vol. 65, no. 4, pp. 1094-1102, April 2017.

5. J. Bito, S. Jeong and M. M. Tentzeris, "A Real-Time Electrically Controlled Active Matching Circuit Utilizing Genetic Algorithms for Wireless Power Transfer to Biomedical Implants," in IEEE Transactions on Microwave Theory and Techniques, vol. 64, no. 2, pp. 365-374, Feb. 2016.

6. S. Kim, S. Jeong, J. Bito, A. Georgiadis and M. M. Tentzeris, “A Flexible RF energy harvester using a hybrid printing technology for ‘stand-alone’ wireless sensor platforms,” Flexible and Printed Electronics 2018.

6.2.2 Refereed Conference Proceedings

1. S. Jeong, J. Bito and M. M. Tentzeris, “Design of a Novel Wireless Power System Using Machine Learning Techniques for Drone Applications,” 2016 IEEE Wireless Power Transfer Conference (WPTC), Taipei, 2017, pp. 1-4.

2. S. Jeong, T. Lin, and M. M. Tentzeris, “Range-adaptive Impedance Matching of Wireless Power Transfer Systems Using a Machine Learning Strategy Based on Neural Networks,” Microwave Symposium (IMS), 2015 IEEE MTT-S International, Boston, MA, 2019.

3. J. Bito, S. Jeong and M. M. Tentzeris, “A real-time electrically controlled active matching circuit utilizing genetic algorithms for biomedical WPT applications,” 2015 IEEE Wireless Power Transfer Conference (WPTC), Boulder, CO, 2015, pp.

4. J. Bito, S. Jeong and M. M. Tentzeris, “Heuristic passive and active matching circuit design method for wireless power transfer for moving objects,” 2016 IEEE Wireless Power Transfer Conference (WPTC), Aveiro, 2016, pp. 1-4.

5. S. Kim, J. Bito, S. Jeong, A. Georgiadis and M. M. Tentzeris, “A flexible hybrid printed RF energy harvester utilizing catalyst-based copper printing technologies for far-field RF energy harvesting applications,” Microwave Symposium (IMS), 2015 IEEE MTT-S International, Phoenix, AZ, 2015, pp. 1-4.

6. M. Ote, S. Jeong, and M. M. Tentzeris, “Foreign Object Detection for Wireless Power

Transfer Based on Machine Learning," 2020 IEEE Wireless Power Transfer Conference (WPTC), Seoul, Korea. (Accepted)

REFERENCES

[1] N. Tesla, *Apparatus for transmitting electrical energy.* US Patent 1,119,732, 1914.

[2] M. Catrysse, B. Hermans, and R. Puers, "An inductive power system with integrated bi-directional data-transmission," *Sensors and Actuators A: Physical*, vol. 115, no. 2-3, pp. 221–229, 2004.

[3] A. Kurs, A. Karalis, R. Moffatt, J. D. Joannopoulos, P. Fisher, and M. Soljačić, "Wireless power transfer via strongly coupled magnetic resonances," *Science*, vol. 317, no. 5834, pp. 83–86, 2007. eprint: `http://science.sciencemag.org/content/317/5834/83.full.pdf`.

[4] J. O. Mur-Miranda, G. Fanti, Y. Feng, K. Omanakuttan, R. Ongie, A. Setjoadi, and N. Sharpe, "Wireless power transfer using weakly coupled magnetostatic resonators," *Proc. IEEE ECCE*, pp. 4179–4186, 2010.

[5] T. Imura and Y. Hori, "Maximizing air gap and efficiency of magnetic resonant coupling for wireless power transfer using equivalent circuit and neumann formula," *IEEE Transactions on industrial electronics*, vol. 58, no. 10, pp. 4746–4752, 2011.

[6] X. Wei, Z. Wang, and H. Dai, "A critical review of wireless power transfer via strongly coupled magnetic resonances," *energies*, vol. 7, no. 7, pp. 4316–4341, 2014.

[7] R. E. Hamam, A. Karalis, J. Joannopoulos, and M. Soljačić, "Efficient weakly-radiative wireless energy transfer: An eit-like approach," *Annals of Physics*, vol. 324, no. 8, pp. 1783 –1795, 2009.

[8] C. Chen, T. Chu, C. Lin, and Z. Jou, "A study of loosely coupled coils for wireless power transfer," *IEEE Transactions on Circuits and Systems II: Express Briefs*, vol. 57, no. 7, pp. 536–540, 2010.

[9] S. Cheon, Y. Kim, S. Kang, M. L. Lee, J. Lee, and T. Zyung, "Circuit-model-based analysis of a wireless energy-transfer system via coupled magnetic resonances," *IEEE Transactions on Industrial Electronics*, vol. 58, no. 7, pp. 2906–2914, 2011.

[10] F. Zhang, S. A. Hackworth, W. Fu, C. Li, Z. Mao, and M. Sun, "Relay effect of wireless power transfer using strongly coupled magnetic resonances," *IEEE Transactions on Magnetics*, vol. 47, no. 5, pp. 1478–1481, 2011.

[11] J. Kim, H. Son, K. Kim, and Y. Park, "Efficiency analysis of magnetic resonance wireless power transfer with intermediate resonant coil," *IEEE Antennas and Wireless Propagation Letters*, vol. 10, pp. 389–392, 2011.

[12] C. K. Lee, W. X. Zhong, and S. Y. R. Hui, "Effects of magnetic coupling of nonadjacent resonators on wireless power domino-resonator systems," *IEEE Transactions on Power Electronics*, vol. 27, no. 4, pp. 1905–1916, 2012.

[13] W. Zhong, C. K. Lee, and S. Y. R. Hui, "General analysis on the use of tesla's resonators in domino forms for wireless power transfer," *IEEE Transactions on Industrial Electronics*, vol. 60, no. 1, pp. 261–270, 2013.

[14] B. Wang, T. Nishino, and K. Teo, "Wireless power transmission efficiency enhancement with metamaterials," in *2010 IEEE International Conference on Wireless Information Technology and Systems*, 2010, pp. 1–4.

[15] A. Kurs, R. Moffatt, and M. Soljačić, "Simultaneous mid-range power transfer to multiple devices," *Applied Physics Letters*, vol. 96, no. 4, p. 044 102, 2010. eprint: https://doi.org/10.1063/1.3284651.

[16] W. X. Zhong, C. K. Lee, and S. Y. Hui, "Wireless power domino-resonator systems with noncoaxial axes and circular structures," *IEEE Transactions on Power Electronics*, vol. 27, no. 11, pp. 4750–4762, 2012.

[17] A. P. Sample, D. T. Meyer, and J. R. Smith, *Analysis, experimental results, and range adaptation of magnetically coupled resonators for wireless power transfer*, 2011.

[18] W. Fu, B. Zhang, and D. Qiu, "Study on frequency-tracking wireless power transfer system by resonant coupling," in *2009 IEEE 6th International Power Electronics and Motion Control Conference*, 2009, pp. 2658–2663.

[19] T. P. Duong and J. Lee, "Experimental results of high-efficiency resonant coupling wireless power transfer using a variable coupling method," *IEEE Microwave and Wireless Components Letters*, vol. 21, no. 8, pp. 442–444, 2011.

[20] G. Lee, B. H. Waters, Y. G. Shin, J. R. Smith, and W. S. Park, "A reconfigurable resonant coil for range adaptation wireless power transfer," *IEEE Transactions on Microwave Theory and Techniques*, vol. 64, no. 2, pp. 624–632, 2016.

[21] J. Lee, Y. Lim, H. Ahn, J. Yu, and S. Lim, "Impedance-matched wireless power transfer systems using an arbitrary number of coils with flexible coil positioning," *IEEE Antennas and Wireless Propagation Letters*, vol. 13, pp. 1207–1210, 2014.

[22] H. Qiu, Y. Narusue, Y. Kawahara, T. Sakurai, and M. Takamiya, "Digital coil: Transmitter coil with programmable radius for wireless powering robust against distance

variation," in *2018 IEEE Wireless Power Transfer Conference (WPTC)*, 2018, pp. 1–4.

[23] T. C. Beh, M. Kato, T. Imura, S. Oh, and Y. Hori, "Automated impedance matching system for robust wireless power transfer via magnetic resonance coupling," *IEEE Trans. Ind. Electron.*, vol. 60, no. 9, pp. 3689–3698, 2012.

[24] B. H. Waters, A. P. Sample, and J. R. Smith, "Adaptive impedance matching for magnetically coupled resonators," in *Proceedings of the PIERS*, Citeseer, 2012.

[25] J. Kim and J. Jeong, "Range-adaptive wireless power transfer using multiloop and tunable matching techniques," *IEEE Transactions on Industrial Electronics*, vol. 62, no. 10, pp. 6233–6241, 2015.

[26] J. Bito, S. Jeong, and M. M. Tentzeris, "A real-time electrically controlled active matching circuit utilizing genetic algorithms for wireless power transfer to biomedical implants," *IEEE Transactions on Microwave Theory and Techniques*, vol. 64, no. 2, pp. 365–374, 2016.

[27] Y. Li, W. Dong, Q. Yang, J. Zhao, L. Liu, and S. Feng, "An automatic impedance matching method based on the feedforward-backpropagation neural network for a wpt system," *IEEE Transactions on Industrial Electronics*, vol. 66, no. 5, pp. 3963–3972, 2019.

[28] N. Oodachi, K. Ogawa, H. Kudo, H. Shoki, S. Obayashi, and T. Morooka, "Efficiency improvement of wireless power transfer via magnetic resonance using transmission coil array," in *2011 IEEE International Symposium on Antennas and Propagation (APSURSI)*, 2011, pp. 1707–1710.

[29] T. Imura, T. Uchida, and Y. Hori, "Flexibility of contactless power transfer using magnetic resonance coupling to air gap and misalignment for ev," *World Electric Vehicle Journal*, vol. 3, no. 2, pp. 332–341, 2009.

[30] T. Kumagai, K. Saito, M. Takahashi, and K. Ito, "Design of receiving antenna for microwave power transmission to capsular endoscope," in *2011 IEEE MTT-S International Microwave Workshop Series on Innovative Wireless Power Transmission: Technologies, Systems, and Applications*, 2011, pp. 145–148.

[31] S. Kim, J. S. Ho, L. Y. Chen, and A. S. Y. Poon, "Wireless power transfer to a cardiac implant," *Applied Physics Letters*, vol. 101, no. 7, p. 073 701, 2012. eprint: https://doi.org/10.1063/1.4745600.

[32] A. Mittleider, B. Griffin, and C. Detweiler, "Experimental analysis of a uav-based wireless power transfer localization system," in *Experimental Robotics: The 14th International Symposium on Experimental Robotics*, M. A. Hsieh, O. Khatib, and

V. Kumar, Eds. Cham: Springer International Publishing, 2016, pp. 357–371, ISBN: 978-3-319-23778-7.

[33] A. R. Koelle, S. W. Depp, and R. W. Freyman, "Short-range radio-telemetry for electronic identification, using modulated rf backscatter," *Proceedings of the IEEE*, vol. 63, no. 8, pp. 1260–1261, 1975.

[34] K. Finkenzeller, *RFID Handbook: Fundamentals and Applications in Contactless Smart Cards and Identification*. 2003.

[35] S. Preradovic, I. Balbin, N. C. Karmakar, and G. Swiegers, "A novel chipless rfid system based on planar multiresonators for barcode replacement," in *2008 IEEE International Conference on RFID*, 2008, pp. 289–296.

[36] C. S. Hartmann, "A global saw id tag with large data capacity," in *2002 IEEE Ultrasonics Symposium, 2002. Proceedings.*, vol. 1, 2002, 65–69 vol.1.

[37] D. Girbau, A. Lázaro, and Ramos, "Time-coded chipless rfid tags: Design, characterization and application," in *2012 IEEE International Conference on RFID-Technologies and Applications (RFID-TA)*, 2012, pp. 12–17.

[38] S. Preradovic and N. C. Karmakar, "Low cost chipless rfid systems," in *Multiresonator-Based Chipless RFID: Barcode of the Future*. New York, NY: Springer New York, 2012, pp. 9–24, ISBN: 978-1-4614-2095-8.

[39] D. Dominic, S. Krafft, N. Safdari, and S. Bhadra, "Multiresonator-based printable chipless rfid for relative humidity sensing," *Proceedings*, vol. 1, no. 4, 2017.

[40] S. Preradovic and N. C. Karmakar, "Design of short range chipless rfid reader prototype," in *2009 International Conference on Intelligent Sensors, Sensor Networks and Information Processing (ISSNIP)*, 2009, pp. 307–312.

[41] S. Preradovic, I. Balbin, N. C. Karmakar, and G. F. Swiegers, "Multiresonator-based chipless rfid system for low-cost item tracking," *IEEE Transactions on Microwave Theory and Techniques*, vol. 57, no. 5, pp. 1411–1419, 2009.

[42] P. Kalansuriya, N. C. Karmakar, and E. Viterbo, "On the detection of frequency-spectra-based chipless rfid using uwb impulsed interrogation," *IEEE Transactions on Microwave Theory and Techniques*, vol. 60, no. 12, pp. 4187–4197, 2012.

[43] W. Dullaert, L. Reichardt, and H. Rogier, "Improved detection scheme for chipless rfids using prolate spheroidal wave function-based noise filtering," *IEEE Antennas and Wireless Propagation Letters*, vol. 10, pp. 472–475, 2011.

[44] A. Vena, E. Perret, and S. Tedjini, "Chipless rfid tag using hybrid coding technique," *IEEE Transactions on Microwave Theory and Techniques*, vol. 59, no. 12, pp. 3356–3364, 2011.

[45] L. M. Arjomandi, G. Khadka, Z. Xiong, and N. C. Karmakar, "Document verification: A cloud-based computing pattern recognition approach to chipless rfid," *IEEE Access*, vol. 6, pp. 78 007–78 015, 2018.

[46] S. Preradovic, I. Balbin, N. C. Karmakar, and G. F. Swiegers, "Multiresonator-based chipless rfid system for low-cost item tracking," *IEEE Transactions on Microwave Theory and Techniques*, vol. 57, no. 5, pp. 1411–1419, 2009.

[47] P. Kalansuriya, N. C. Karmakar, and E. Viterbo, "On the detection of frequency-spectra-based chipless rfid using uwb impulsed interrogation," *IEEE Transactions on Microwave Theory and Techniques*, vol. 60, no. 12, pp. 4187–4197, 2012.

[48] M. A. Hearst, S. T. Dumais, E. Osuna, J. Platt, and B. Scholkopf, "Support vector machines," *IEEE Intelligent Systems and their Applications*, vol. 13, no. 4, pp. 18–28, 1998.

[49] S. B. Kotsiantis, I Zaharakis, and P Pintelas, "Supervised machine learning: A review of classification techniques," *Emerging artificial intelligence applications in computer engineering*, vol. 160, pp. 3–24, 2007.

[50] M. A. Friedl and C. E. Brodley, "Decision tree classification of land cover from remotely sensed data," *Remote sensing of environment*, vol. 61, no. 3, pp. 399–409, 1997.

[51] J. R. Quinlan, "Learning efficient classification procedures and their application to chess end games," in *Machine learning*, Springer, 1983, pp. 463–482.

[52] M.-H. Chiu, Y.-R. Yu, H. Liaw, and L. Chun-Hao, "The use of facial micro-expression state and tree-forest model for predicting conceptual-conflict based conceptual change," Jan. 2016.

[53] N. S. Altman, "An introduction to kernel and nearest-neighbor nonparametric regression," *The American Statistician*, vol. 46, no. 3, pp. 175–185, 1992.

[54] A. Bronshtein. (2017). A quick introduction to k-nearest neighbors algorithm.

[55] G. J. McLachlan, *Discriminant analysis and statistical pattern recognition*. John Wiley & Sons, 2004, vol. 544.

[56] V. N. Vapnik, *Statistical Learning Theory*. Wiley-Interscience, 1998.

[57] JavaTpoint. (2011). Classification of neural network in tensorflow.

[58] L. A. Gatys, A. S. Ecker, and M. Bethge, "A neural algorithm of artistic style," *arXiv preprint arXiv:1508.06576*, 2015.

[59] Ansaro. (2017). Interpreting machine learning models.

[60] T. C. Beh, M. Kato, T. Imura, S. Oh, and Y. Hori, "Automated impedance matching system for robust wireless power transfer via magnetic resonance coupling," *IEEE Transactions on Industrial Electronics*, vol. 60, no. 9, pp. 3689–3698, 2013.

[61] B. Park and J. Lee, "Adaptive impedance matching of wireless power transmission using multi-loop feed with single operating frequency," *IEEE Transactions on Antennas and Propagation*, vol. 62, no. 5, pp. 2851–2856, 2014.

[62] K.-I. Funahashi, "On the approximate realization of continuous mappings by neural networks," *Neural Networks*, vol. 2, no. 3, pp. 183 –192, 1989.

[63] S. Jeong, T. Lin, and M. M. Tentzeris, "A real-time range-adaptive impedance matching utilizing a machine learning strategy based on neural networks for wireless power transfer systems," *IEEE Transactions on Microwave Theory and Techniques*, vol. 67, no. 12, pp. 5340–5347, 2019.

[64] J. Shin, S. Shin, Y. Kim, S. Ahn, S. Lee, G. Jung, S. Jeon, and D. Cho, "Design and implementation of shaped magnetic-resonance-based wireless power transfer system for roadway-powered moving electric vehicles," *IEEE Transactions on Industrial Electronics*, vol. 61, no. 3, pp. 1179–1192, 2014.

[65] Chiuk Song, Hongseok Kim, D. H. Jung, Kibum Yoon, Yeonje Cho, Sunkyu Kong, Younghwan Kwack, and Joungho Kim, "Three-phase magnetic field design for low emi and emf automated resonant wireless power transfer charger for uav," in *2015 IEEE Wireless Power Transfer Conference (WPTC)*, 2015, pp. 1–4.

[66] M. J. Rosenberg and R. Foshay, "E-learning: Strategies for delivering knowledge in the digital age," *Performance Improvement*, vol. 41, no. 5, pp. 50–51, 2002. eprint: `https://onlinelibrary.wiley.com/doi/pdf/10.1002/pfi.4140410512`.

[67] M. Mohri, A. Rostamizadeh, and A. Talwalkar, *Foundations of machine learning*. MIT press, 2018.

[68] E. Alpaydin, *Introduction to machine learning*. MIT press, 2009.

[69] S. Jeong, J. Bito, and M. M. Tentzeris, "Design of a novel wireless power system using machine learning techniques for drone applications," in *2017 IEEE Wireless Power Transfer Conference (WPTC)*, 2017, pp. 1–4.

[70] S. Amendola, R. Lodato, S. Manzari, C. Occhiuzzi, and G. Marrocco, "RFID technology for IoT-based personal healthcare in smart spaces," *IEEE Internet of Things Journal*, vol. 1, no. 2, pp. 144–152, 2014.

[71] K. Yamano, K. Tanaka, M. Hirayama, E. Kondo, Y. Kimuro, and M. Matsumoto, "Self-localization of mobile robots with rfid system by using support vector machine," in *2004 IEEE/RSJ International Conference on Intelligent Robots and Systems (IROS)*, vol. 4, 2004, pp. 3756–376.

[72] T. Hofmann, B. Schölkopf, and A. J. Smola, "Kernel methods in machine learning," *The annals of statistics*, pp. 1171–1220, 2008.

[73] D. Girbau, J. Lorenzo, A. Lazaro, C. Ferrater, and R. Villarino, "Frequency-coded chipless rfid tag based on dual-band resonators," *IEEE Antennas Wireless Propag. Lett.*, vol. 11, pp. 126–128, 2012.

[74] F. Costa, S. Genovesi, and A. Monorchio, "Normalization-free chipless rfids by using dual-polarized interrogation," *IEEE Trans. Microw. Theory Techn.*, vol. 64, no. 1, pp. 310–318, 2015.

[75] L. M. Arjomandi and N. C. Karmakar, "An enhanced chipless rfid system in 60 ghz using pattern recognition techniques," in *2018 48th European Microwave Conference (EuMC)*, 2018, pp. 973–976.

[76] A. Ramos, E. Perret, O. Rance, S. Tedjini, A. Lázaro, and D. Girbau, "Temporal separation detection for chipless depolarizing frequency-coded rfid," *IEEE Trans. Microw. Theory Techn.*, vol. 64, no. 7, pp. 2326–2337, 2016.

[77] A. Vena, E. Perret, and S. Tedjni, "A depolarizing chipless rfid tag for robust detection and its fcc compliant uwb reading system," *IEEE transactions on microwave theory and techniques*, vol. 61, no. 8, pp. 2982–2994, 2013.

[78] F. Babaeian and N. Karmakar, "A cross-polar orientation insensitive chipless rfid tag," in *2019 IEEE International Conference on RFID Technology and Applications (RFID-TA)*, IEEE, 2019, pp. 116–119.

[79] S. Jeong, J. G. Hester, W. Su, and M. M. Tentzeris, "Read/interrogation enhancement of chipless rfids using machine learning techniques," *IEEE Antennas and Wireless Propagation Letters*, vol. 18, no. 11, pp. 2272–2276, 2019.